

AD-A080 423

AIR FORCE INST OF TECH WRIGHT-PATTERSON AFB OH SCHOO--ETC F/8 17/5
OPTICAL RECEIVER DESIGN USING PYROELECTRIC DETECTORS.(U)

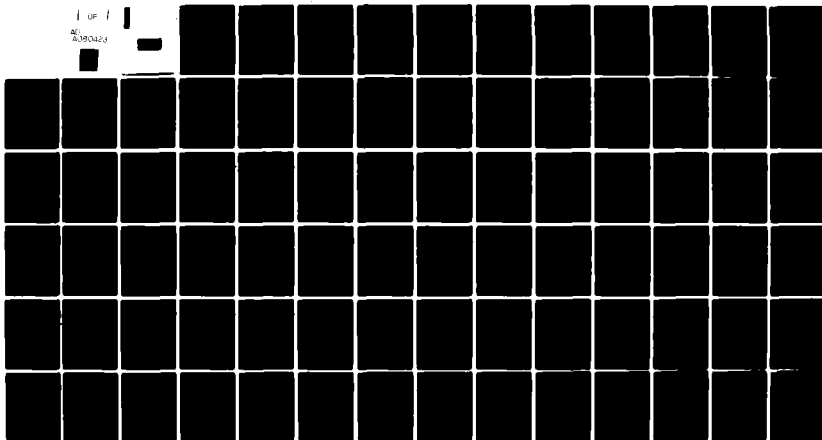
DEC 79 M J GOODMAN

AFIT/8EO/EE/79-2

UNCLASSIFIED

NL

1 OF 1
AD-A080 423



END
DATE
FILMED
3-80
DOC

6 OPTICAL RECEIVER DESIGN
USING PYROELECTRIC DETECTORS

9 Master THESIS,

James

14 AFIT/GEC/EE/79-2

10 Michael ~~Goodman~~
2nd Lt USAF

11 Dec 79

12 82

1980

Approved for public release; distribution unlimited.

012225

mit

OPTICAL RECEIVER DESIGN
USING PYROELECTRIC DETECTORS

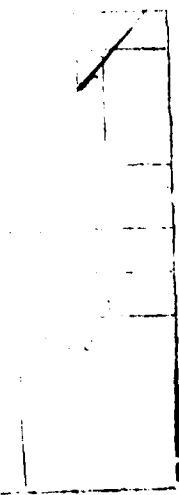
THESIS

Presented to the Faculty of the School of Engineering
of the Air Force Institute of Technology
Air University
in Partial Fulfillment of the
Requirements for the Degree of
Master of Science

by
Michael J. Goodman, B.S.
2nd Lt USAF
Graduate Electrical Engineering
December 1979

Approved for public release; distribution unlimited.

A



Preface

The pyroelectric detector has different characteristics than photon detectors used in quantum receivers. Consequently, it hasn't been until recently that receiver design using a pyroelectric element as the detector has been considered. The present emphasis is mainly attributed to the growing need for an uncooled thermal detector which can respond favorably under adverse conditions.

Recent developments in receiver design have been made to produce a solid-state pyroelectric detector array (Ref 22). However, fundamental problems such as sensitivity, spatial resolution, heat loading of the solid-state substrate and a technologically feasible fabrication technique had to be overcome. In this work I don't claim any contributions to those problems, however, I do present a means of optimally processing a signal transduced by a single point detector from noise generated by the detector. This contribution to the receiver design is a practical application of frequency equalization of the detector response.

The presentation of material covered provides only the main parameters influencing the radiation transduction to the output signal. There are some areas such as the derivation of the dielectric loss tangent and approximation of the electrical time constant which have not been clearly stated in the literature. I attempt to clarify the derivations in the appendices by introducing approximations essential to agreement with results confirmed in the literature. However, not all results in the literature are accurate. As an example Vander Ziel (Ref 31) describes a noise current spectral density which, without clarification, is incorrect. This mistake is noted and an accurate clarification is stated in chapter IV.

The bibliography does not include every reference, obviously. However, a review of work done in pyroelectricity has been compiled in a "Literature Guide to Pyroelectricity," by Lang (Ref 13). Putley (Ref 20;21) presents the pyroelectric in a developmental role and a design for a frequency compensated detector.

I want to thank my thesis advisor, Capt Stanley R. Robinson, for his patience and suggestions during the thesis development. I also want to thank Dr. Theodore E. Luke, my faculty advisor, and Major Joseph Carl for their comments and review of the draft. I also thank Diana Hudson for typing the draft. Most of all, I thank the Lord for His mercy, patience, love, and grace shown toward us all (Matthew 11:28-30).

Michael J. Goodman

Table of Contents

	Page
Preface.	ii
List of Figures.	vi
List of Tables	viii
List of Symbols.	ix
Abstract	xii
I. Introduction	1
Objective	1
Background.	2
II. Pyroelectric Detector Properties	5
Pyroelectric Effect	6
Crystal Symmetries.	6
Pyroelectric Detector	7
Material Conductance & Dielectric Loss Factor	10
Summary	12
III. Detector Signal Model.	13
Thermal Responsivity.	13
Detector Load-Preamplifier.	17
Voltage Mode	18
Current Mode	21
Model Performance	22
Summary	24
IV. Detector Noise Model	29
Detector Noise Sources.	29
Temperature-Fluctuation Noise.	29
Dielectric Loss Noise.	30
Amplifier Noise Sources	32
Load Thermal Noise	32
Gate Current Noise	32
Amplifier Noise Voltage.	32
Noise Equivalent Circuit.	33
Summary	33

Table of Contents

(Cont'd)

	Page
V. Noise Filtering & Signal Response.	36
Pyroelectric Detector Sensor Unit SNR	36
Noise Filter Network.	37
Whitening Filter	37
Matched Filter	39
Filter Output	40
Summary	41
VI. Conclusion	42
Bibliography	44
Appendix A: Material Conductance & Dielectric Loss Factor . .	47
Appendix B: Electrical Time Constant.	50
Appendix C: Detector Signal Response.	52
Vita	66

List of Figures

Figure		Page
1	Pyroelectric Detector Electrode.	8
2	Pyroelectric Detector Normalized Responsivity.	16
3	Pyroelectric Detector Block Diagram.	16
4	Pyroelectric Detector Equivalent Circuit with Load Resistance	17
5	Voltage Mode Detector Equivalent Circuit	18
6	Pyroelectric Detector-Preamplifier Frequency Spectrum. .	20
7	Current Mode Detector Equivalent Circuit	22
8	Pyroelectric Detector-Preamplifier Output Voltage for $T_e > T_{TH}$	25
9	Pyroelectric Sensor Output Voltage for $T_{TH} > T_e$	26
10	Pyroelectric Sensor Output Voltage due to a Pulse Train. .	27
11	Temperature-Fluctuation Noise Power Spectral Density . .	31
12	Composite Noise Equivalent Circuit	34
13	Block Diagram of the Optical Receiver.	38
B-1	Voltage Mode R-C Network	51
B-2	Current Mode R-C Network	51
C-1	Pyroelectric Sensor Output Voltage due to a Step Signal for $T_{TH} > T_e$	55
C-2	Pyroelectric Sensor Output Voltage due to a Step Signal for $T_e > T_{TH}$	56
C-3	Pyroelectric Sensor Output Voltage due to a Pulse for $T_{TH} > T_e$ and $t_o > t_p$	57
C-4	Pyroelectric Sensor Output Voltage due to a Pulse for $T_{TH} > T_e$ and $t_p > t_o$	58
C-5	Pyroelectric Sensor Output Voltage due to a Pulse for $T_e > T_{TH}$ and $t_o > t_p$	59
C-6	Pyroelectric Sensor Output Voltage due to a Pulse for $T_e > T_{TH}$ and $t_p > t_o$	60

List of Figures

(Cont'd)

Figure		Page
C-7	Pyroelectric Sensor Output Voltage due to a Pulse Train with a 50% duty cycle for $T_{TH} > T_e$ and $t_o > t_p$	61
C-8	Pyroelectric Sensor Output Voltage due to a Pulse Train with a 95% duty cycle for $T_{TH} > T_e$ and $t_o > t_p$	62
C-9	Pyroelectric Sensor Output Voltage due to a Pulse Train with a 50% duty cycle for $T_e > T_{TH}$ and $t_o > t_p$	63
C-10	Pyroelectric Sensor Output Voltage due to a Pulse Train with a 75% duty cycle for $T_e > T_{TH}$ and $t_o > t_p$	64
C-11	Pyroelectric Sensor Output Voltage due to a Pulse Train with a 90% duty cycle for $T_e > T_{TH}$ and $t_o > t_p$	65

List of Tables

Table	Page
I. Detector Parameters.	4
II. Pyroelectric Crystalline Properties.	7

List of Symbols

<u>Symbol</u>	<u>Quantity</u>	<u>Unit</u>
A	Sensitive Detector Area	cm ²
a _v	Preamplifier Gain	v/v
b	Detector Thickness	cm
C	Specific Heat	J/°K
C _T	Thermal Capacity	J/°K
C _d , C _e , C _f , C _o	Detector, Equivalent, Feedback, Preamplifier Input Capacitance, Respectively	F
C ^E	Volume Specific Heat	J/cm ³ °K
D	Electric Displacement Vector	V _m
E	Electric Field Vector	v/m
e	Electric Charge	J
f, f _o	Electrical, Modulation Frequency Respectively	Hz
F _o	Flux or Radiant Power	W
F(t)	Instantaneous Radiant Power	W
g _d	Detector Conductance	$\frac{1}{\Omega}$
g _R	Radiative Loss Conductance per Unit Area	w/cm ² °K
H(f)	Circuit Transfer Function	-
I	Pyroelectric Current	Amp
I _{go,1,2}	Preamplifier Gate Current	Amp
k	Boltzmann Constant	J/°K
NEP	Noise Equivalent Power	-
P	Polarization Vector	Asec/m ²
P _s	Spontaneous Polarization	Asec/m ²
Q	Heat Flow into Crystal	J/cm ³

List of Symbols

(Cont'd)

<u>Symbol</u>	<u>Quantity</u>	<u>Unit</u>
R	Resistance	Ω
R_d, R_e, R_f, R_l, R_i	Detector, Equivalent, Feedback, Load, Input Resistance, Respectively	Ω
R_n	Equivalent Noise Resistance	Ω
IR	Responsivity	v/w
IR_i, IR_v	Current, Voltage Responsivity	I/w, v/w
S	Entropy	J/K
S_i, S_v	Noise Current & Voltage Power Density	$A^2 \cdot sec, v^2 \cdot sec$
s	Density	gm/cm ³
SNR	Signal-to-Noise Ratio	-
T, T_c	Ambient-Sample, Curie Temperature	$^{\circ}K$
T_e, T_{TH}	Electrical, Thermal Time Constant	sec
V	Pyroelectric Voltage	volt
V_o, V_{out}, V_s, V_w	Filter Output Voltages	volt
Z_f	Feedback Impedance	Ω
ϵ	Dielectric Permittivity	(Asec) ² /Ncm ²
ϵ_o	Free Space Permittivity	(Asec) ² /Ncm ²
σ	Stephan Boltzmann Constant	w/m ² $^{\circ}K^4$
σ_e	Electrical Conductivity	1/ Ωm
σ_n^2	Average Noise Power	volt ²
λ	Pyroelectric Coefficient	C/cm ² $^{\circ}K$
η	Emissivity	-
ρ	Surface Charge	Amp sec/m ²
χ	Susceptibility	-

List of Symbols

(Cont'd)

<u>Symbol</u>	<u>Quantity</u>	<u>Unit</u>
$\tan\delta$	Dielectric Loss Tangent	-
$\phi(t)$	Random Fluctuation in Power Exchanged Between the Detector and its Surroundings	Watts

Abstract

An optical receiver operable over a broad spectral range of the infrared region is possible using a pyroelectric point detector. The pyroelectric detector is modeled as a transducer of thermal radiation to an electrical signal cascaded with an R-C network. The pyroelectric signal is amplified by a preamplifier network. The sensor is, therefore, modeled as a linear bandpass filter.

The preamplifier is configured in two modes, the voltage mode which limits the response to a narrow electrical bandwidth, and the current mode which broadens the response over a wide electrical bandwidth. The responsivity bandwidth product is dependent upon the preamplifier components determined by the mode of operation. However, pulse widths and pulse repetition rates can be calculated without regard to mode of operation.

The detector performance is theoretically limited by fluctuations of the incident radiation and is practically constrained by the thermally generated noise within the preamplifier components. The optical receiver signal processing consists of a whitening filter cascaded with a matched filter. The filter network is used to optimally process the sensor output. The processing scheme provides a signal-to-noise improvement of 10^6 over straight detection.

OPTICAL RECEIVER DESIGN USING PYROELECTRIC DETECTORS

I. Introduction

The pyroelectric detector transduces incident infrared radiation into an electrical signal. The electrical signal may be amplified by a network and processed by filtering noise effects from the detector output. The combination of detector, preamplifier, and filtering network constitute what is defined as the optical receiver in this thesis. The front end of the receiver, such as the lens system and spectral filters, are omitted from the receiver design. The detector-pre-amplifier combination is defined as the sensor and the filtering network may be referred to as the post detection processor. The post detection processor is used to equalize the frequency response of the noise power density so as to utilize matched filtering techniques.

Objectives

The objectives of the design include: (1) presentation of the operating characteristics of pyroelectrics, by analyzing equivalent circuit models, noise sources, and different operating configurations; (2) examine a post detection processing scheme to measure such parameters as narrow pulse widths, pulse energy, and pulse repetition rate; (3) determine optimum post detection processing to estimate the parameters previously mentioned and to include noise effects on computing measurement accuracy; and (4) comment on the design complexity. Each objective presented is dependent upon the ability to describe the radiation transduction characteristics of the detector.

Background

In an article Lin & Long (Ref 15) present a comprehensive review of the pyroelectric detector and the materials used for such detectors. The presentation treats both the ideal and practical pyroelectric detector. However, the practical detector responsivity is described by the heat transfer through various layers of materials used in the transducers, whereas, the ideal detector is described merely by the thermal properties of the pyroelectric. Another review of pyroelectric detectors is presented by Putley (Ref 20;21). The description of the detector is given by including the equivalent preamplifier network with the detector and denoting the response as that of the pyroelectric detector. In such an analysis the thermally generated noise within the resistive element does not distinguish between dielectric loss and the load resistance noise sources.

The description of the noise sources in pyroelectric detectors is presented by Vander Ziel (Ref 31). In the presentation the noise sources present in the pyroelectric detector include: (1) radiation noise, (2) temperature-fluctuation noise, (3) detector thermal noise, (4) load thermal noise, (5) gate noise of the preamplifier, and (6) amplifier voltage noise. There exists an inconsistency in Vander Ziel's definition of the detector thermal noise and noise power density definitions. That inconsistency can only be corrected when it is stated that the loss tangent is inversely proportional with frequency over the range of interest. The temperature-fluctuation and dielectric loss (detector thermal noise) noise sources are equivalent when the pyroelectric is a low loss material as presented by Stokowski (Ref 28). The analysis is rather complicated, however, it assumes that the

dielectric constant is small.

The response of the pyroelectric detector is analyzed by Peterson, et al. (Ref 18). The magnitude of the detector response is plotted for various materials and parameters. The response dependence upon temperature change is accomplished by modulating the incident radiation at frequencies greater than 10 Hz.

There are several articles found in literature related to various aspects of the pyroelectric detector. The most significant articles previously mentioned have been used to develop what follows as the presentation of the pyroelectric detector application in an optical receiver. The parameter values used consistently throughout the text are given in Table I, for a pyroelectric element made of Triglycine Sulphate (TGS).

The pyroelectric detector properties are described in Chapter Two. In Chapter Three, the sensor responsivity is defined. Chapter Four, presents the noise sources generated within the sensor unit and the noise filtering network is presented in Chapter Five.

Table I
Detector Parameters

<u>Symbol</u>		<u>Value</u>
A	Sensitive Detector Area	10^{-2} cm^2
b	Detector Thickness	$25 \times 10^{-4} \text{ cm}$
$C_T = C^E b A$	Thermal Capacitance	$6.25 \times 10^{-5} \text{ J/}^\circ\text{K}$
$C_d = \epsilon_R \epsilon_0 A/b$	Detector Capacitance	12.39 pF
C^E	Volume Specific Heat	$2.5 \text{ J/cm}^3 \text{ }^\circ\text{K}$
ϵ_R	Radiative Loss Conductance per Unit Area	$6.10 \times 10^{-4} \frac{\text{W}}{\text{cm}^2 \text{ }^\circ\text{K}}$
I_{go}	Preamplifier Gate Current	10^{-17} Amp
T	Ambient-Material Temperature	300°K
T_C	Curie Temperature	322°K
T_{TH}	Thermal Time Constant	10.2 sec
ϵ_R	Relative Dielectric Permittivity	35
λ	Pyroelectric Coefficient	$4 \times 10^{-8} \text{ Asec/cm}^2 \text{ }^\circ\text{K}$
k	Boltzmann Constant	$1.38 \times 10^{-23} \text{ J/}^\circ\text{K}$
σ	Stephan-Boltzmann Constant	$5.67 \times 10^{-12} \text{ W/cm}^2 \text{ }^\circ\text{K}^4$
ϵ_0	Free Space Permittivity	$8.854 \times 10^{-8} \frac{(\text{Amp sec})^2}{\text{N} \cdot \text{cm}^2}$
e	Electric Charge	$1.602 \times 10^{-19} \text{ Amp sec}$

II. Pyroelectric Detector Properties

The pyroelectric detector response to thermal radiation is dependent upon the pyroelectric effect. The detectors electrical properties are related to the thermodynamic properties of the crystalline material by the pyroelectric coefficient. Pyroelectricity is described physically as the change with temperature of positive and negative polarization charges along a unique polarization axis of crystals belonging to the noncentrosymmetric classes (Ref 4). Mathematically, pyroelectricity is a relation between a scalar (temperature) and a vector (polarization). When the crystal is held motionless (clamped), the effect observed is called primary pyroelectricity. With free expansion of the crystal there is an additional effect called secondary pyroelectricity due to the piezoelectric nature of the pyroelectric. The combination of the primary and the secondary effects is observed as an external electric field.

Pyroelectric materials or pyroelectrics are a class of piezoelectric materials which exhibit an alteration of the material polarization due to small changes in temperature. Pyroelectrics have a non-zero polarization, even when the applied external field or applied stress is zero, referred to as the spontaneous polarization. A polarization may be produced in some crystals by a hydrostatic pressure (Ref 16:78), which is a special case of the piezoelectric effect. In some pyroelectrics, changes of applied field can reduce the polarization to zero and reverse it. This reversal of the polarization is characteristic of the subgroup of pyroelectric materials called Ferroelectrics (Ref 3). It is assumed that the pyroelectric is used at an ambient temperature much less than the Curie temperature. Excessive heat tends to destroy the

ferroelectric order and, at the Curie point, the crystal changes to an unpolarized state.

Pyroelectric Effect

If the temperature change is uniform over an isotropic crystal, then the pyroelectric effect is described by a pyroelectric coefficient vector $\bar{\lambda}$,

$$\Delta \bar{P} = \bar{\lambda} \Delta T \quad (1)$$

where \bar{P} is the polarization vector and T is the temperature. An external electric field will not normally be observed (Ref 20), since if the material is a conductor, its mobile charge carriers will assume a distribution which neutralizes the internal moment, while if it is an insulator, stray charges will be attracted to and trapped on the surfaces until the surface charge associated with the polarization is neutralized. The charge distribution produced in this way near the surface of an insulator is relatively stable, unable to respond quickly to sudden changes of the internal dipole moment. Thus, in particular, if the temperature of the material is changed, the dipole moment may also change, and this change will produce an observable external electric field.

Crystal Symmetries

Pyroelectric materials are noncentrosymmetrical crystals having a unique axis along which the spontaneous polarization exists. Among the 32-point group symmetries of crystalline solids, 21 are noncentrosymmetric classes, 10 of which can exhibit spontaneous polarization (triclinic, 1; monoclinic, m and 2; orthorhombic, $2mm$; trigonal, 3 and $3m$; tetragonal, 4 and $4mm$; and hexagonal, 6 and $6mm$). Nye (Ref 16) clarifies which

axis direction the polarization vector may exist. In point group 1 the vector $\vec{\lambda}$ is not determined by symmetry and it has three nonzero components in a rectangular coordinate system. In point group m, symmetry requires $\vec{\lambda}$ to lie in the mirror plane and it has two nonzero components. In the other eight point groups, symmetry requires $\vec{\lambda}$ to lie parallel to the unique rotational axis. In these point groups, therefore, $\vec{\lambda}$ has only one nonzero component. The most important pyroelectric crystals studied seriously for detector applications belong to the latter eight point groups. Examples of common pyroelectrics are given in Table II.

Table II
Pyroelectric Crystalline Properties

Material	Pyroelectric Coefficient ($\text{Ccm}^{-1}\text{K}^{-1}$)	Point Group < T_C	Curie Temperature T_C (°K)	Ref
Tourmaline	4×10^{-10}	3m		(20)
Triglycine-Sulphate (TGS) ($\text{NH}_2\text{CH}_2\text{COOH}$) $_3\text{H}_2\text{SO}_4$	4×10^{-8}	2	322	(15)
Lithium Tantalate (LiT_2O_3)	1.9×10^{-8} 6×10^{-9}	3m		(15) (20)
Strontium-Barium-Niobate (SBN)	6.0×10^{-8}	4mm		(15)
Polyvinylidene Fluoride (PVF $_2$)	0.3×10^{-8}	2mm		(15)

Pyroelectric Detector

Most practical point pyroelectric detectors are made of thin wafers of pyroelectric crystals. The polarization of the crystal is oriented so that it is normal to the two electroded surfaces as shown in Figure 1. (The arrow indicating the polarization direction is shown

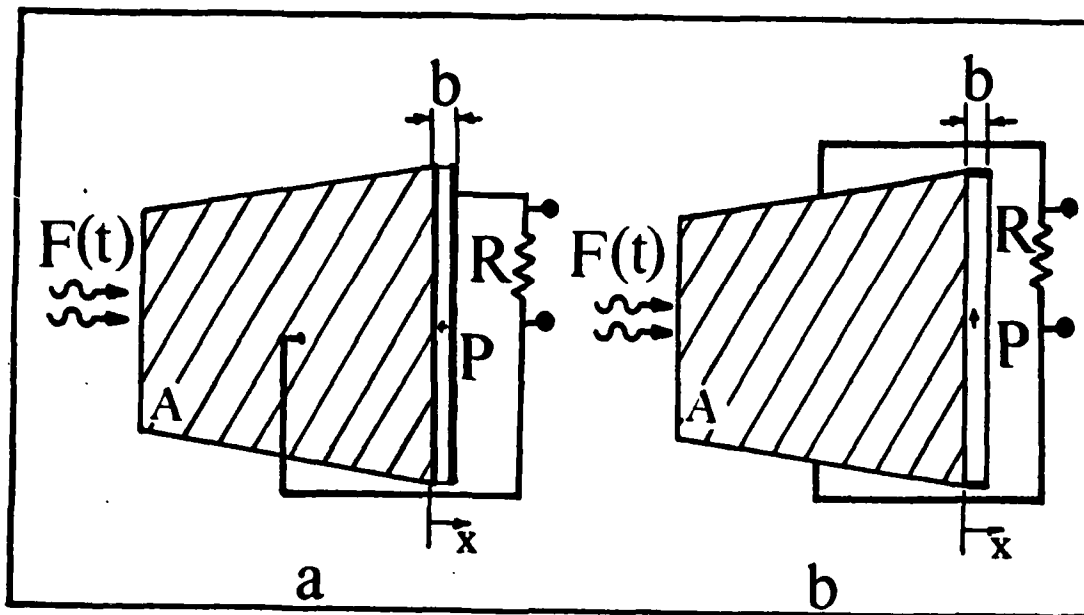


Figure 1. Pyroelectric Detector Electrode Configuration a) Face Electrode, b) Edge Electrode.

within the material). Both the face electrode and the edge electrode configurations form a parallel-plate capacitor, modelling the detector as a circuit element. For the face electrode, a gold-black (Ref 1) coating may be used as the electrode material while also increasing the detector responsivity. However, for the edge electrode configuration the only function of the surface coating is to increase detector responsivity.

If \vec{P} is the polarization (dipole per unit volume), both spontaneous and induced, of the pyroelectric it may be related to the macroscopic electric displacement by

$$\vec{D}(t) = \epsilon_0 \vec{E}(t) + \vec{P}(t) \quad (2)$$

where \vec{E} is the electric field vector, ϵ_0 is the free space permittivity, and $\nabla \cdot \vec{D} = \rho$, where ρ is the bound surface charge of the material.

Since $\nabla \cdot \mathbf{E} = \frac{\rho}{\epsilon_0} - \frac{\nabla \cdot \mathbf{P}}{\epsilon_0}$ it follows that the electric field vector is due not only to the real charge ρ , but also exists where $\nabla \cdot \mathbf{P} \neq 0$ (at such a point there is said to be a polarization charge). Under constant conditions real charge ρ eventually accumulates at points where $\nabla \cdot \mathbf{P} \neq 0$ and thus neutralizes the dipole field. A change of temperature or stress will change the permanent lattice polarization and flow of charge will neutralize the new value of $\nabla \cdot \mathbf{P}$ at a rate determined by the electric conductivity. In this case the current set up in the external circuit (the pyroelectric current) is required to be related to the input radiation flux.

Consider the electrode arranged in Figure 1(a), where the ferroelectric domains have been oriented in an electric field to give the polarization vector \mathbf{P} in the direction between the electrodes, i.e., in the x-direction. When the displacement current is included the current density J in the x direction of the pyroelectric is:

$$J = \sigma_{\text{ex}} E_x + \frac{\partial D_x}{\partial t} \quad (3)$$

where σ_{ex} is the electrical conductivity. However, \mathbf{P} is a function of \mathbf{E} , so that if X_x is the susceptibility, and P_{xs} is the spontaneous polarization, then

$$P_x = P_{xs} + X_x E_x \quad (4)$$

The equation of continuity requires that $\nabla \cdot \mathbf{J} = 0$, or in this case $\frac{\partial J}{\partial x} = 0$. Hence, J is a function of t only and is independent of x .

Substitution of equation 4 into equation 3 yields,

$$J(\mathbf{E}) = \sigma_{\text{ex}} E_x + \frac{\partial}{\partial t} (\epsilon E_x + P_{xs}) \quad (5)$$

where $\epsilon = \epsilon_0 (1 + X_x)$ is the dielectric constant. The total current flowing out of the pyroelectric if the electrodes have a sensitive area

A is

$$I = AJ = \sigma_{ex} E_x A + \frac{\partial}{\partial t} (\epsilon E_x A) + \frac{\partial}{\partial t} P_{xs} A \quad (6)$$

Notice when $\vec{E} = 0$, the pyroelectric crystal still shows a polarization and

$$I = \frac{\partial}{\partial t} P_{xs} A = A \frac{\partial P_{xs}}{\partial \Delta T} \frac{\partial \Delta T}{\partial t} \quad (7)$$

where $\frac{\partial P_{xs}}{\partial \Delta T} = \lambda_x$ is defined as the pyroelectric coefficient. From equation 7, if the temperature is constant in time then $I = 0$. Therefore, only a change in temperature produces an observable electrical signal.

Material Conductance & Dielectric Loss Factor

The detector electrode configuration is used to determine the electrical capacitance of the pyroelectric, however, the electrical conductance remains to be determined. The electrical and thermoconductivities can be related by state equations (Ref 16). The relationship between the electrical, thermal, and mechanical properties are described by three principal effects. However, when an isotropic crystal is clamped the relationship between electrical and thermal properties is described by the heat capacity, the permittivity, and the coupling effect of pyroelectricity. The state equations showing the differential change of the crystal entropy is described by

$$dS = \lambda_i dE_i + (C^E/T)dT \quad (8)$$

where the subscripts denote vector components and the differential change of the electric displacement is given by

$$dD_i = \epsilon dE_i + \lambda_i dT \quad (9)$$

where D_i , E_i , S , and T are the displacement field components, electric field components, entropy, and temperature respectively. The coefficients

ϵ , λ_i , and C^E are the dielectric permittivity, pyroelectric coefficient, and heat capacity at constant electric field. By manipulating the above state equations and applying the second law of thermodynamics the relationship between the thermoconductivity and the material electrical conductance can be determined. The derivation is presented in Appendix A; the resulting expression for the conductance of the pyroelectric, for a lossy material, in the frequency domain is given as

$$g_d = \frac{(\lambda \ 2\pi f)^2 \ T_A}{g_R (1 + (2\pi f \ T_{TH})^2)} \quad (10)$$

where $T_{TH} = C^E b / g_R$, the thermal response time (dielectric relaxation time), and $g_R = 4\eta\sigma T^3$, where η is the emissivity, and σ is the Stephan Boltzmann constant. For $2\pi f \gg 1/T_{TH}$, $g_d = \lambda^2 T_A / g_R T_{TH}^2$ and for $T_{TH} = 10.2$ sec the $g_d = 7.56 \times 10^{-14} \frac{1}{\Omega}$. Notice that T_{TH} is dependent upon the material thickness, therefore, given a material with thickness $b = 1 \mu m$, $T_{TH} = 0.408$ sec. When T_{TH} is small the condition $2\pi f \gg 1/T_{TH}$ in which case the material conductance is assumed constant. Notice that for $2\pi f \ll 1/T_{TH}$ the conductance is not linear, however, the requirement states that for linearity to exist $2\pi f \gg 1/T_{TH}$ must be satisfied.

The dielectric loss can also be derived, based upon the definition of g_d , and is given as

$$\tan\delta = \frac{\lambda^2 \ T \ 2\pi f \ b}{\epsilon_R \epsilon_O (1 + (2\pi f \ T_{TH})^2) g_R} \quad (11)$$

where ϵ_R is constant over the range of frequencies of interest and $\tan\delta \sim 2.66 \times 10^{-22} \frac{1}{f}$ for $2\pi f \gg 1/T_{TH}$. Therefore, the material conductance is constant over frequencies greater than the thermal response frequency, and the loss tangent is inversely proportional with frequency

over this range.

Summary

With a uniform change of temperature the pyroelectric effect can be described by the mathematical relationship between the polarization vector and the temperature of the material. Only 10 noncentrosymmetric crystals have a unique axis along which polarization may occur exhibiting spontaneous polarization. The relationship between the macroscopic electric displacement and polarization determine the polarization-temperature relationship of the pyroelectric effect.

The dielectric losses of the pyroelectric are described by the differential changes in the macroscopic electrical and thermodynamic properties. However, since the losses are small the dielectric permittivity may be assumed constant. The relationship between the electrical and thermal conductivities is also given by the pyroelectric coupling effect. The pyroelectric detector can physically be modeled as a current source in parallel connection with a capacitance and a loss resistance which is approximately constant for all frequencies. To describe the nature of the detector response to incident radiation it is necessary to obtain a solution to a heat flow equation. In the next chapter, the solution is used to describe the relationship of the incident radiation and the output electrical signal.

III. Detector Signal Model

When the pyroelectric detector absorbs a time-varying radiation its temperature rises, changing its surface charge, and developing an electrical response across the detector capacitance. The detector will respond to any spectrum of radiation from warm objects, cold objects, or laser sources, as long as the radiation is absorbed and converted into heat to change the temperature of the pyroelectric.

A common approach of describing the detector characteristics is by a response transfer function due to modulated radiation (Ref 20; Ref 15). Modulation of the incident radiation can be accomplished with a chopper (Ref 24; Ref 10) or by pulsating the radiation from the source. The modulation may be sinusoidal (Ref 20), step-like (Ref 26), or rectangular pulses (Ref 24). The response transfer function is found by solving a heat equation (Ref 5) with appropriate initial and boundary conditions.

Thermal Responsivity

In order to calculate the thermal responsivity, the rate of temperature change dT/dt , of the crystal has to be known. The thermal properties can be described by the differential equation of conduction of heat in an isotropic solid with a source term due to the absorption of radiation by the crystal (Ref 5:9)

$$C^E_{bA} \frac{dT}{dt} = \eta F(t) - g_R A \Delta T \quad (12)$$

where $F(t)$ = incident modulated radiation
 C^E = Volume specific heat at constant E
 g_R = radiative loss conductance per unit area

T = change in surface temperature

A = sensitive detector area

b = detector thickness

η = emissivity

The first term on the right-hand side represents the temperature rise due to illumination and the second term describes the heat losses in the device. The term on the left-hand side is the transient temperature variation with time. The total incident radiation power $F(t)$ is uniformly received by a pyroelectric wafer with emissivity, equivalent to the absorptivity, of approximately unity. The thermal capacity of the detector, $C_T = C^E b A$, and the thermal conductance, $G_T = g_R A$, can be used to describe the thermal response time. For a detector it is desirable that C_T be low and G_T be made as small as possible.

The solution to equation 12 can be obtained by using frequency domain techniques assuming the thermal capacity and conductance as constant parameters. The steady-state solution for T is given as

$$\Delta T(f) = \frac{\eta F(f)}{C_T (1 + j 2\pi f T_{TH})} \quad (13)$$

where $F(f)$ is the frequency domain representation of $F(t)$ and $T_{TH} = \frac{C^E b}{g_R}$ is the thermal time constant. Remember that the detector only responds to a time change in temperature.

As a capacitive device, the surface charge on the electrodes of the detector can be given by

$$\Delta Q(f) = A \Delta P = \lambda A \Delta T(f) \quad (14)$$

producing an open-circuit voltage,

$$\Delta V(f) = \frac{\Delta Q(f)}{C_d} = \frac{\lambda}{\epsilon_R \epsilon_0} b \Delta T(f) \quad (15)$$

where $C_d = \epsilon_0 \epsilon_R \cdot \frac{A}{b}$, is the detector capacitance and ϵ_R is the dielectric constant of the material. The current is given by

$$\Delta I(f) = j2\pi f C_d \Delta V(f) \quad (16)$$

Therefore, from equation 15 and equation 16, respectively, the voltage and current (Ref 31; Ref 8) responsivities are given as (Ref 15), respectively,

$$IR(f) = \frac{\eta \lambda}{C^E \epsilon_R \epsilon_0 A} \frac{T_{TH}}{(1 + j2\pi f T_{TH})} \quad \frac{\text{Volt}}{\text{Watt}} \quad (17)$$

$$IR_i(f) = \frac{\eta \lambda}{C^E b} \frac{j2\pi f T_{TH}}{(1 + j2\pi f T_{TH})} \quad \frac{\text{Amp}}{\text{Watt}} \quad (18)$$

The magnitudes of both responsivities, normalized to unity, are plotted in Figure 2. The voltage responsivity of the detector is determined by the two parameters $\frac{\eta \lambda}{C^E \epsilon_0 \epsilon_R \cdot A}$ and T_{TH} , and the current responsivity by the two parameters $\frac{\eta \lambda}{C^E b}$ and T_{TH} . It is apparent that the voltage response decreases while the current response increases as the frequency increases. It should be noted that the decreasing voltage response is comparable with the dielectric nature of the pyroelectric crystal since the dielectric loss tangent has a similar response.

A block diagram of the transfer of incident radiation through the pyroelectric to yield an output signal is shown in Figure 3 where the pyroelectric voltage and current in the frequency domain are given, respectively, by

$$V(f) = \frac{F(f) \eta \lambda T_{TH}}{C^E C_d b (1 + j2\pi f T_{TH})} \quad (19)$$

and

$$I(f) = \frac{F(f) \eta \lambda j2\pi f T_{TH}}{C^E b (1 + j2\pi f T_{TH})} \quad (20)$$

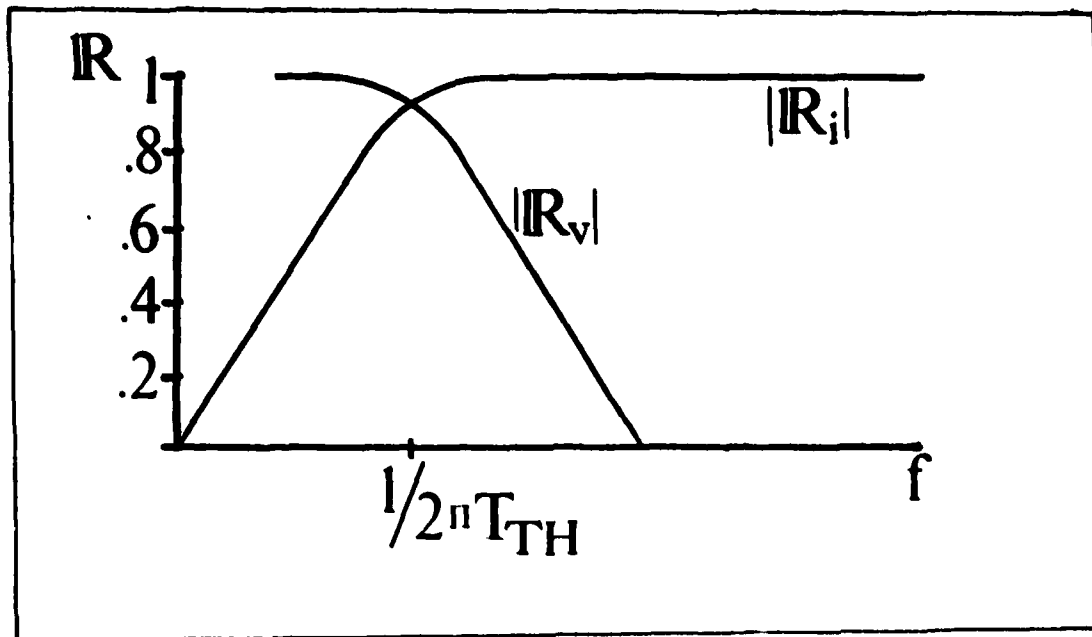


Figure 2. Pyroelectric Detector Normalized Responsivity

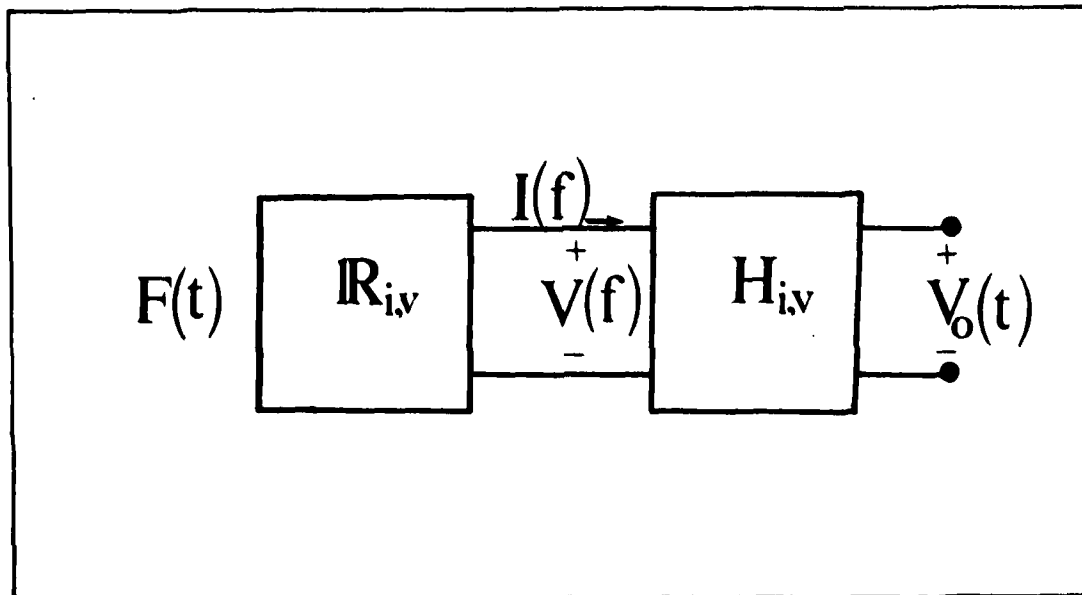


Figure 3. Pyroelectric Detector Block Diagram

where $F(f)$ denotes the Fourier Transform of $F(t)$.

Detector Load - Preamplifier

By applying an external load or a preamplifier to the detector, the electrical bandwidth response may be broadened or narrowed for choice of load value. The load therefore is used to determine the electrical time constant for the detector. Throughout the analysis the electrical time constant is calculated for the preamplifier networks with the distinction between configurations made by subscripting the parameter T_e . The subscripts range from 0 to 3 and are omitted when the general case is inferred.

Consider the case when an external resistance is connected across the detector electrodes, the equivalent circuit is shown in Figure 4.

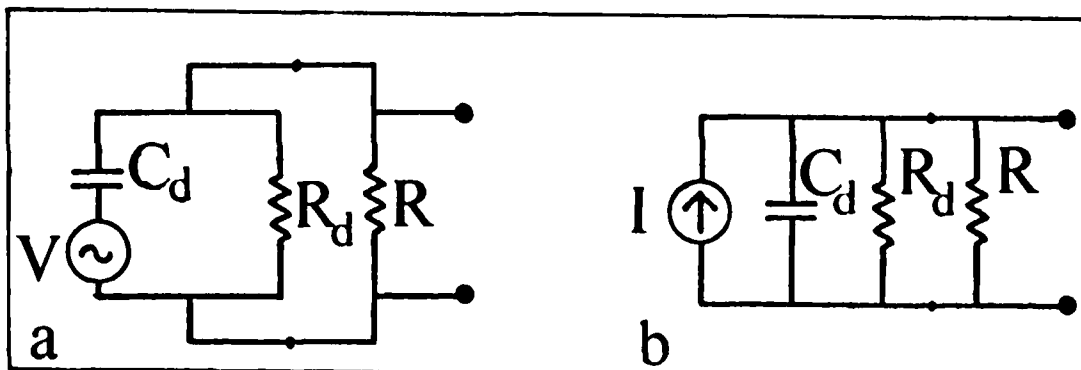


Figure 4. Pyroelectric Detector Equivalent Circuit with Load Resistance a) Thevenin, b) Norton.

For the circuit in Figure 4(a) the voltage transfer response in the frequency-domain is given by

$$V_o(f) = \frac{F(f) j2\pi f \eta \lambda}{C^E C_d b (j2\pi f + 1/T_{TH}) (j2\pi f + 1/T_{eo})} \quad (21)$$

where $T_{eo} = R_d R C_d / (R_d + R) \approx R C_d$ is the electrical time constant.

The approximation is dependent upon $R_d \gg R$. In Appendix B the condition is shown to exist for all frequencies.

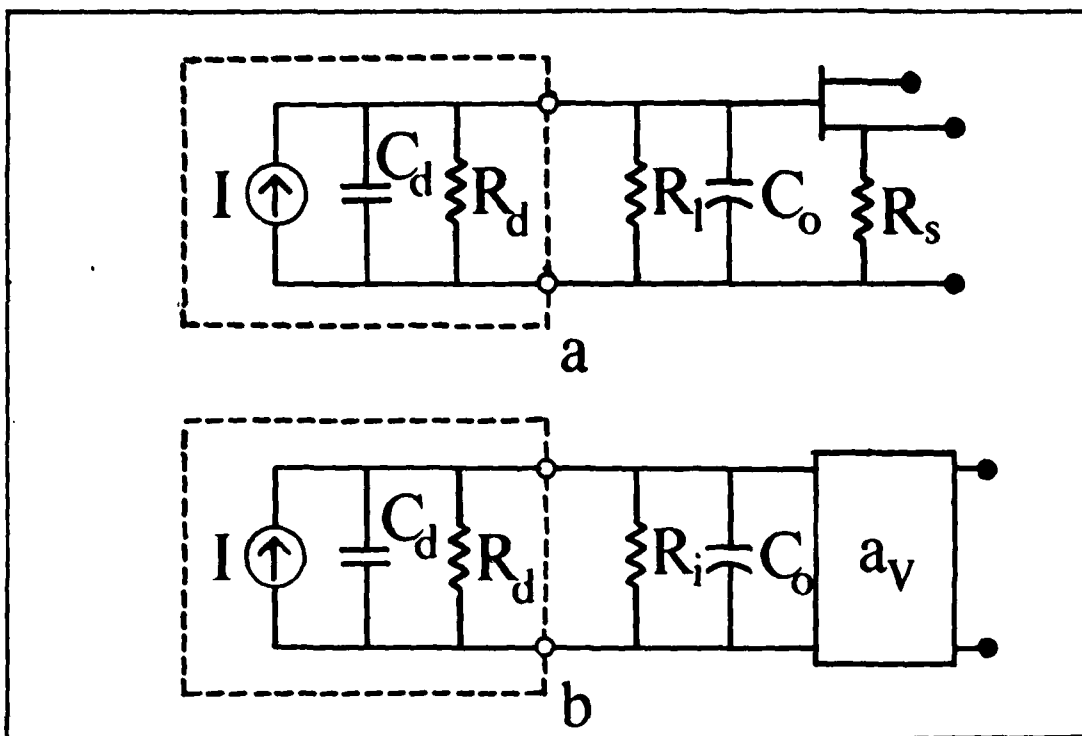


Figure 5. Voltage Mode Detector Equivalent Circuit:
 a) Actual Circuit, b) Equivalent Circuit.

For the current transfer configuration in Figure 4(b), the voltage response in the frequency-domain is also given by equation 21. Therefore, it is apparent that the two transfer responses are Thevenin and Norton equivalences of a capacitive element. However, a voltage and a current mode configuration can be described by the choice of a pre-amplifier network.

Voltage Mode Preamplifier. When operating the high-impedance pyroelectric detector in the voltage mode, a high-impedance field-effect-transistor (FET) is used to sense the voltage across the detector electrodes. The actual circuit is shown in Figure 5(a), where the FET is connected in the source follower configuration, R_d is the load resistance, C_o is the input capacitance, and R_s is the FET source resistance.

The limiting fall off at low frequencies (d.c.) is determined by the pyroelectric material itself when $T_e < T_{TH}$, and by the equivalent FET preamplifier input resistance when $T_{TH} < T_e$. The FET circuit equivalence is analyzed for a mid-frequency range determined by the thermal time constant and the internal capacitance and resistance of the FET (Ref 33). At high frequencies the FET can be described by a hybrid- π equivalent circuit (Ref 23) such that Figure 5(a) is reduced to an equivalent circuit shown in Figure 5(b), where a_v is the voltage gain, V_{out}/V_o , determined by the internal capacitances and conductances, $R_i = r_{ds} || R_s || R_L$ the input resistance, and r_{ds} is the drain-to-source resistance. For an FET $r_{ds} \gg R_s$ so that R_i becomes $R_s || R_L$.

The transfer function for the voltage mode configuration (Ref 20: 264) becomes

$$IR(f) = \frac{j2\pi f \eta \lambda a_v}{C^E C_d b (j2\pi f + 1/T_{TH})(j2\pi f + 1/T_{e1})} \quad (22)$$

where $T_{e1} = R_e C_e = (R_d || R_i)(C_d + C_o)$. For the case when $R_d \gg R_i$ and $C_d \gg C_o$, then $T_{e1} = R_i C_d$ and $T_e < T_{TH}$ so that $IR(f)$ is given as the solid line in Figure 6. The maximum value of responsivity occurs where $\frac{1}{T_{TH}} \ll 2\pi f \ll \frac{1}{T_{e1}}$ and is found to be

$$IR_{max} = \frac{\eta \lambda R_i a_v}{C^E} \quad (23)$$

In the case $2\pi f \gg \frac{1}{T_{e1}}$ and $2\pi f \gg \frac{1}{T_{TH}}$, it follows that

$$IR 2\pi f = \frac{\eta \lambda}{C^E C_e} \quad (24)$$

which is the largest responsivity bandwidth product obtainable from a material using a flat response amplifier. Varying both C^E and C_e result in a trade-off between the responsivity and the bandwidth of the

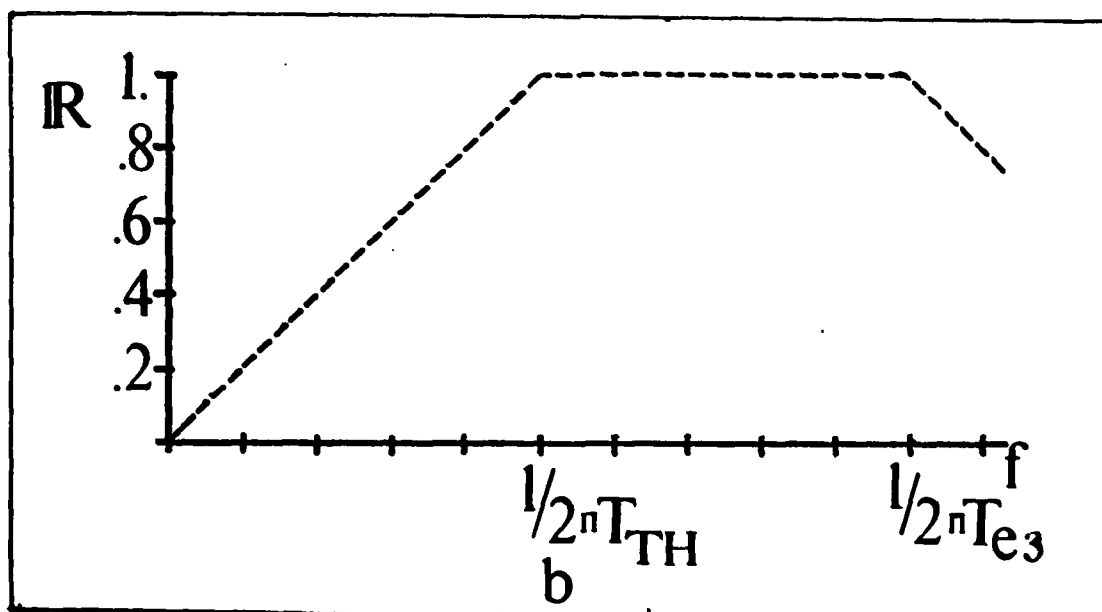
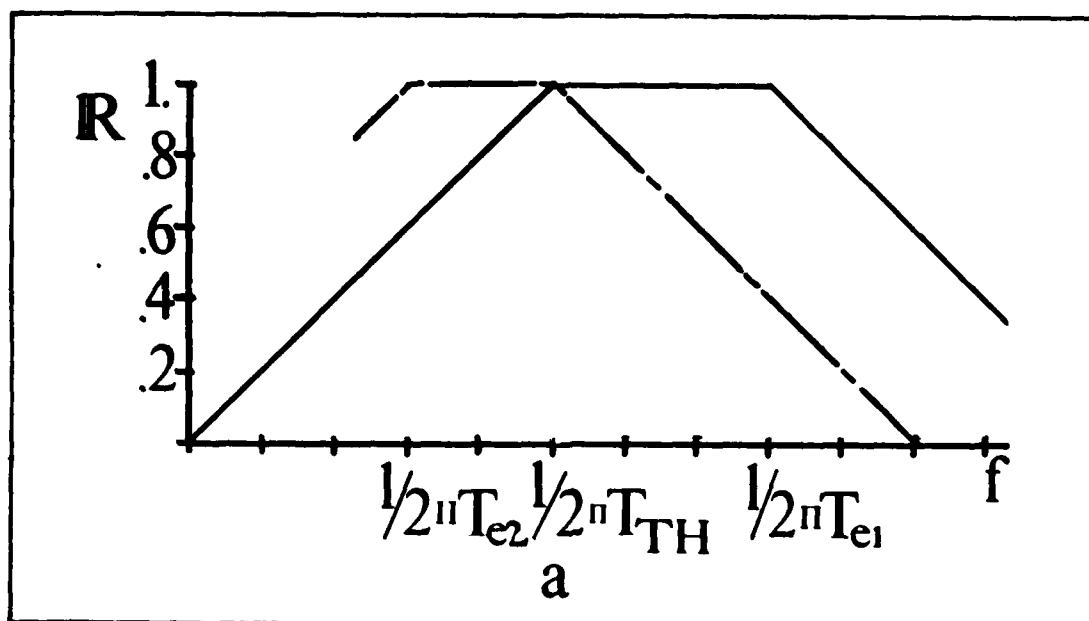


Figure 6. Pyroelectric Detector-Preamplifier Frequency Spectrum

detector. It is important to note that this product is independent of the load resistance. By use of a frequency compensated amplifier, a large $(IR 2\pi f)$ product seems theoretically possible without sacrificing signal-to-noise ratio (Ref 8:163). For the case when $R_d \geq R_l$ or large R_l and $C_d \gg C_o$ then $T_{e2} > T_{TH}$, and $T_{e2} = (R_d || R_l) C_d = R_l C_d$, where the approximation is dependent upon the dielectric nature of the pyroelectric. The maximum value of responsivity, therefore, occurs where $1/T_{e2} \ll 2\pi f \ll 1/T_{TH}$ and is given in equation 23.

Current Mode Preamplifier. When operating the pyroelectric detector in the current mode configuration, it is desirable to detect the change in current produced by the change in temperature. The actual circuit used to monitor the change is shown in Figure 7(a), where C_o is the input capacitance on the operational amplifier having an open loop gain a_v . The operational amplifier is connected in the inverting mode configuration. As a general property of the inverting-amplifier circuit the impedance connected between the input and output appears across the input terminals reduced by the factor 1 plus the voltage gain of the amplifier (known as the Miller-Effect). Therefore, the impedance seen by the detector is reduced significantly lower than R_d (Ref 12:481), Figure 7(b).

The transfer function for the current mode configuration becomes

$$IR(f) = \frac{j2\pi f \eta \lambda a_v}{C^E C_d b (j2\pi f + 1/T_{TH})(j2\pi f + 1/T_{e3})} \quad (25)$$

where $T_{e3} = R_e C_e = (R_d || R_f / (1 + a_v))(C_d + C_o + C_f \cdot (1 + a_v))$. When Z_f is a parallel combination of a feedback resistance and small leakage capacitance, and for the case when $R_d \gg R_f / (1 + a_v)$, $C_d \gg C_o + C_f \cdot (1 + a_v)$, then $T_{e3} = R_f C_d / (1 + a_v)$. Since the voltage gain of an

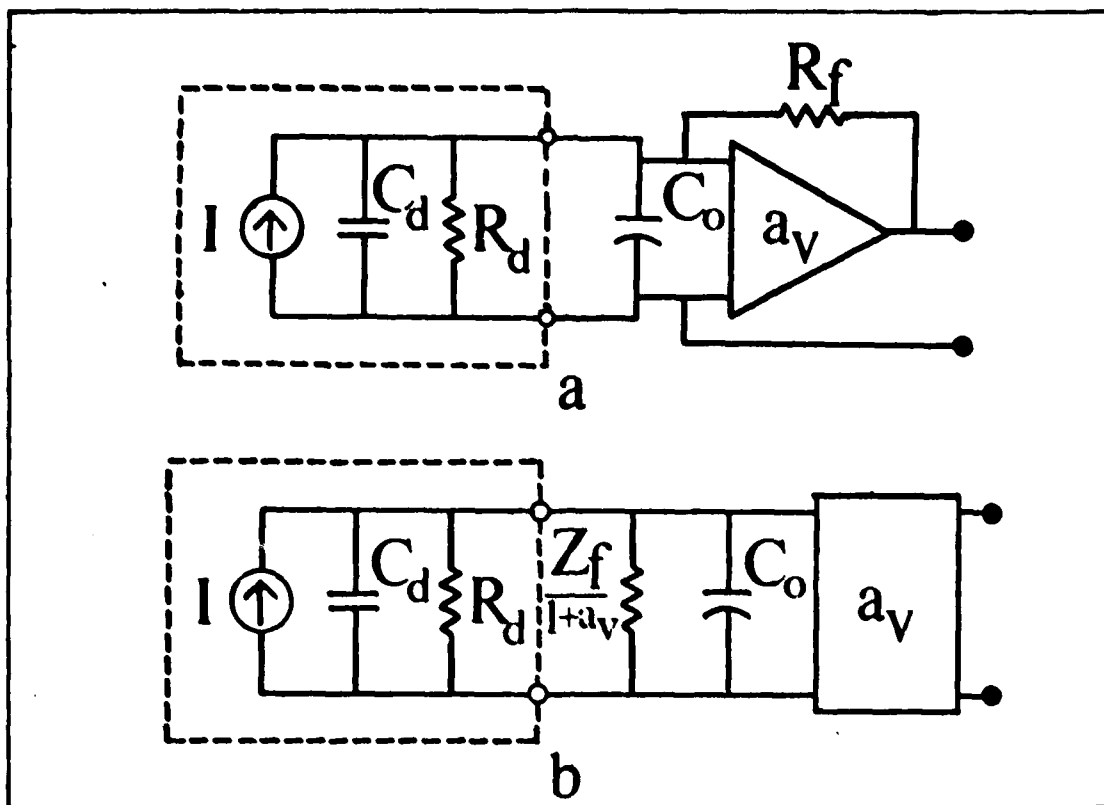


Figure 7. Current Mode Detector Equivalent Circuit:
a) Actual Circuit, b) Equivalent Circuit.

operational amplifier is much greater than 1, $T_{e3} < T_{TH}$ for all practical values of R_f . The transfer response is shown as the dash line in Figure 6, also notice that $R_f/(1 + a_v) < R_i$ so that the current mode response extends further beyond the voltage mode response for $T_{TH} > T_{e2}$.

Model Performance

Analyzing the transfer function given by equation 22 and equation 25, the pyroelectric detector and amplifier can be modeled as a linear bandpass filter. The output voltage response due to an incident radiation pulse of width t_o and amplitude F_o can therefore be given by
(Ref 24:1441)

$$V_{out}(t) = \frac{F_o \eta \lambda a_v}{C^E C_d b \left(\frac{1}{T_e} - \frac{1}{T_{TH}} \right)} \{ (e^{-t/T_{TH}} - e^{-t/T_e}) u(t) - (e^{-(t-t_o)/T_{TH}} - e^{-(t-t_o)/T_e}) u(t-t_o) \} \quad (26)$$

The output voltage for $t < t_o$ is identical to the step-signal response of the detector (Ref 26:3742). The peak value V_p of the response is reached at time $t_p < t_o$,

$$t_p = \frac{T_e T_{TH}}{(T_e - T_{TH})} \ln (T_e/T_{TH}) \quad (27)$$

for $T_e \neq T_{TH}$ is given by

$$V_p = \frac{F_o \eta \lambda a_v T_{TH}}{C^E C_d b} \left(\frac{T_e}{T_{TH}} \right)^{\frac{T_{TH}}{T_{TH} - T_e}} \quad (28)$$

For the case when $T_{TH} \gg T_e$, $V_p = \frac{F_o \eta \lambda a_v T_e}{C^E C_d b}$. For $T_e = RC_d$ and R is small enough for the condition $T_{TH} \gg T_e$ to hold, the peak value of the voltage is proportional to R , and independent of T_{TH} . For $T_e \gg T_{TH}$, on the other hand $V_p = \frac{F_o \eta \lambda a_v T_{TH}}{C^E C_d b}$, so that for a sample with small T_{TH} and/or large R , the peak value of the voltage is proportional to T_{TH} and independent of the load resistance. In any given sample, $\frac{F_o \eta \lambda a_v T_{TH}}{C^E C_d b}$ is the upper limit value of V_p .

Equation 26 can be plotted, for $F_o \cdot a_v \sim$ unity and values for the parameters used given in Table I, for several cases. For the case when $T_e = 0.2864$ sec $\ll T_{TH} = 10.2$ sec and $t_o = 8.0$ sec $> t_p = 1.05$ sec, the rise time T_e is approximately t_p , and the decay time is given as T_{TH} . For the case when $t_o = 1.0$ sec $< t_p = 1.05$ sec, the signal does not reach the maximum peak, however, the peak voltage is given by

$$V_p(t_o) = \frac{F_o \eta \lambda a_v (e^{-t_o/T_{TH}} - e^{-t_o/T_e})}{C^E C_d b \left(\frac{1}{T_e} - \frac{1}{T_{TH}} \right)} \quad (29)$$

occurring at the end of the pulse and shown by the dotted line in Figure 8.

For the case when $T_{TH} = 10.2 \text{ sec} < T_e = 10.2 \text{ sec}$ and $t_o = 32 \text{ sec} > t_p = 26 \text{ sec}$, the rise time T_{TH} is approximately t_p and the decay time is given as T_e . However, $t_p \approx T_{TH}$ presents a long delay time and usually $t_o \ll t_p$. In this case, in Figure 9, the output signal peak is again given as equation 29, and the dotted line represents the case for $t_p = 26 \text{ sec} > t_o = 8.0 \text{ sec}$.

For the case when the incident radiation consists of a pulse train, the response for $T_e = 0.2864 \text{ sec} < T_{TH} = 10.2 \text{ sec}$, $t_o = 8.0 \text{ sec} > t_p = 1.05 \text{ sec}$ and a duty cycle of 50% is shown in Figure 10. The value for $T_e = 0.2864$ requires $R \approx 10^{10} \Omega$ such that the separation between pulses of the response are clearly resolved. The output shown resembles the input pulse train to some degree such that the pulse repetition rate may be measured as the time between pulse peaks. The pulse on-off times t_i and t_f may be obtained such that $t_i = t_p - T_e$ and $t_f = t_p + t_o - T_e$. Therefore, $t_o = t_f - t_i$ and the pulse width is measurable when the positive and negative peaks are observable. A collection of signal responses are found in Appendix C for various duty cycles and pulse widths. Notice that it is possible to obtain a close resemblance of the pulse input for the case when $T_{TH} \gg T_e$ and $t_o > t_p$. Therefore, to obtain an output for pulse width on the order of milliseconds and for $T_{TH} = 10.2 \text{ sec}$ an electrical time constant must be on the order of $1 \times 10^{-5} \text{ sec}$ or say a load resistance of $8 \times 10^{+5} \Omega$.

Summary

The pyroelectric detector can be modeled as a linear bandpass filter. The response of the detector is determined by both the thermal

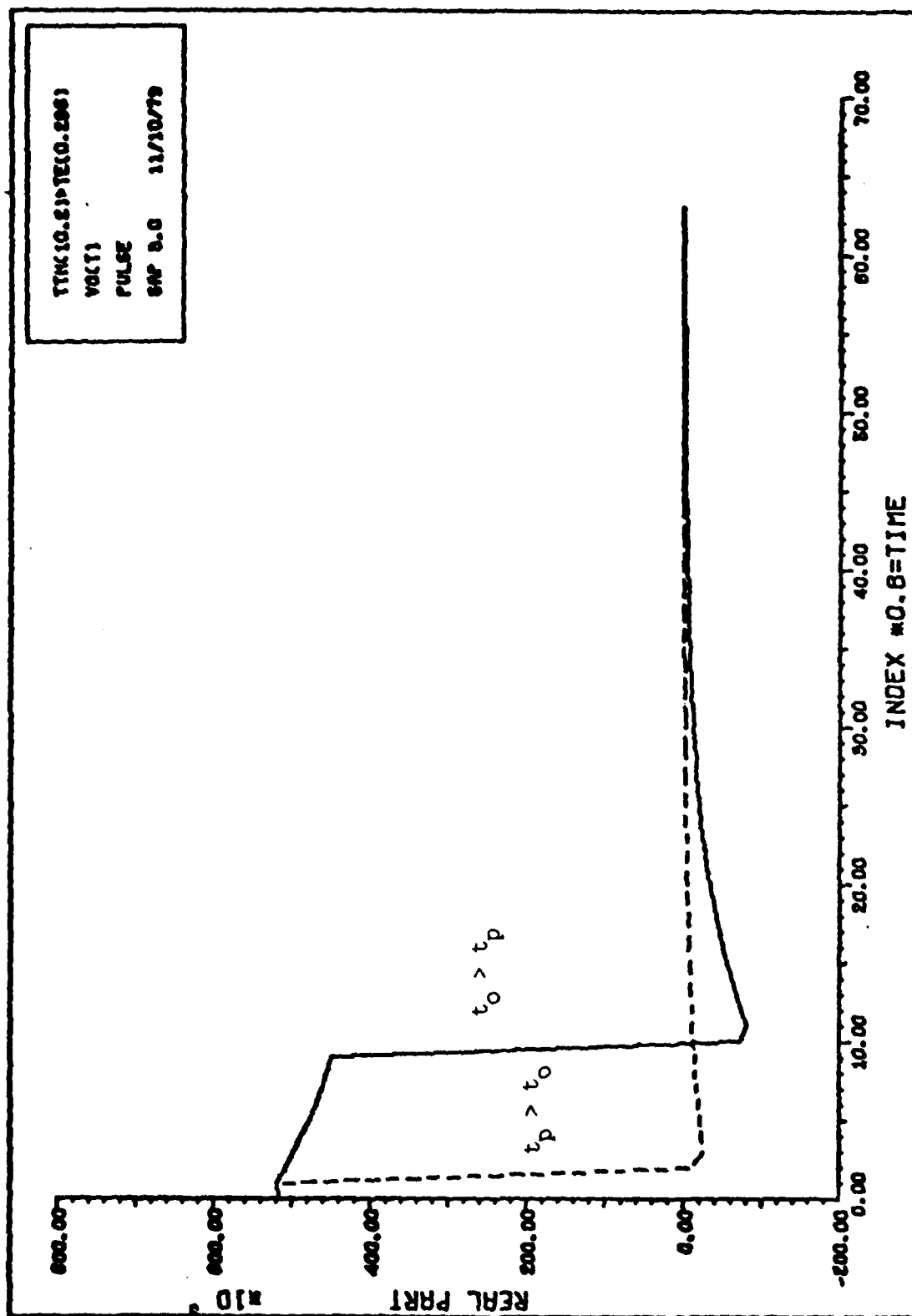


Figure 8. Pyroelectric Detector-Preamplifier Output
Voltage for $T_e > T_{TH}$

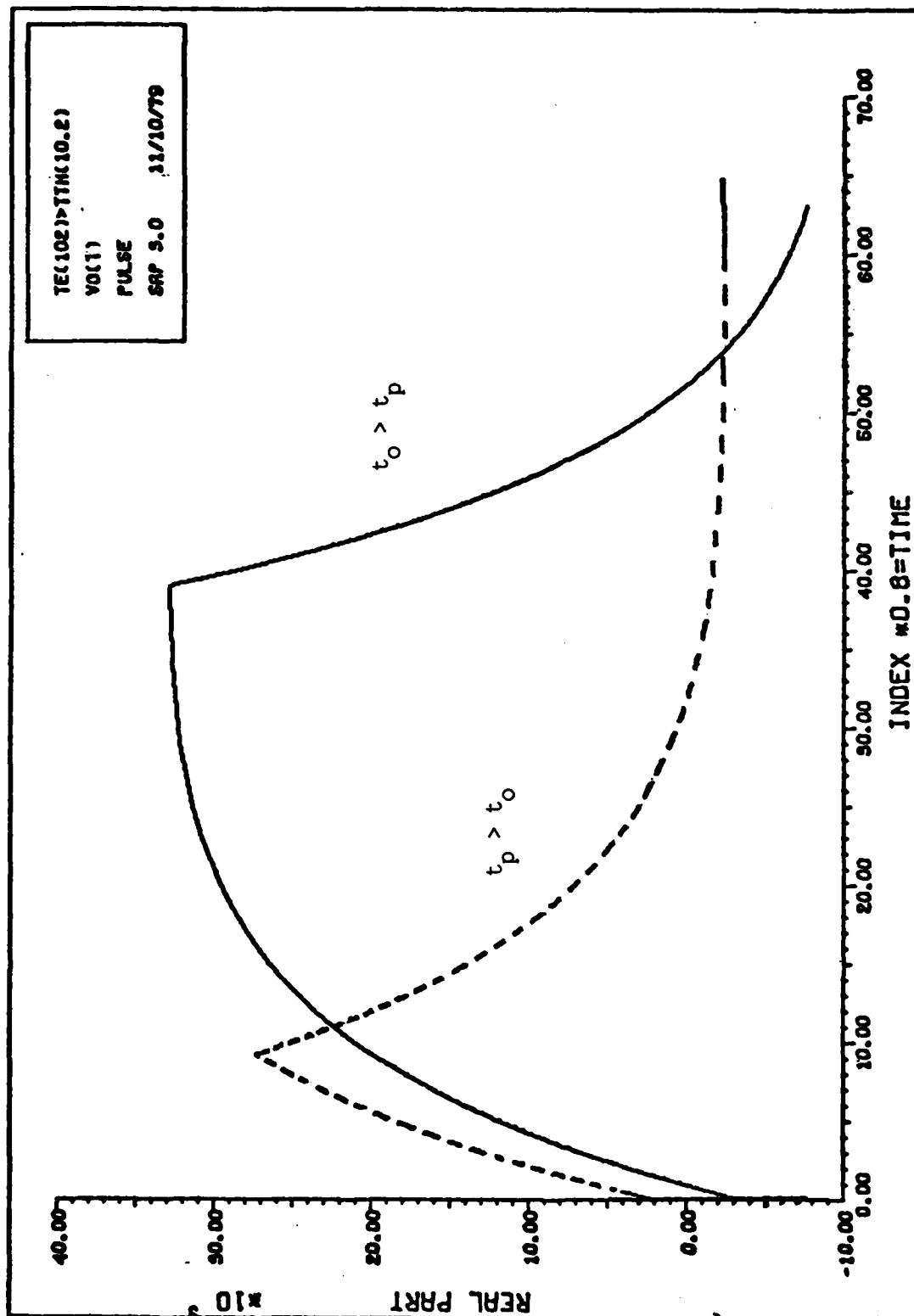


Figure 9. Pyroelectric Sensor Output Voltage for $T_{TH} > T_e$

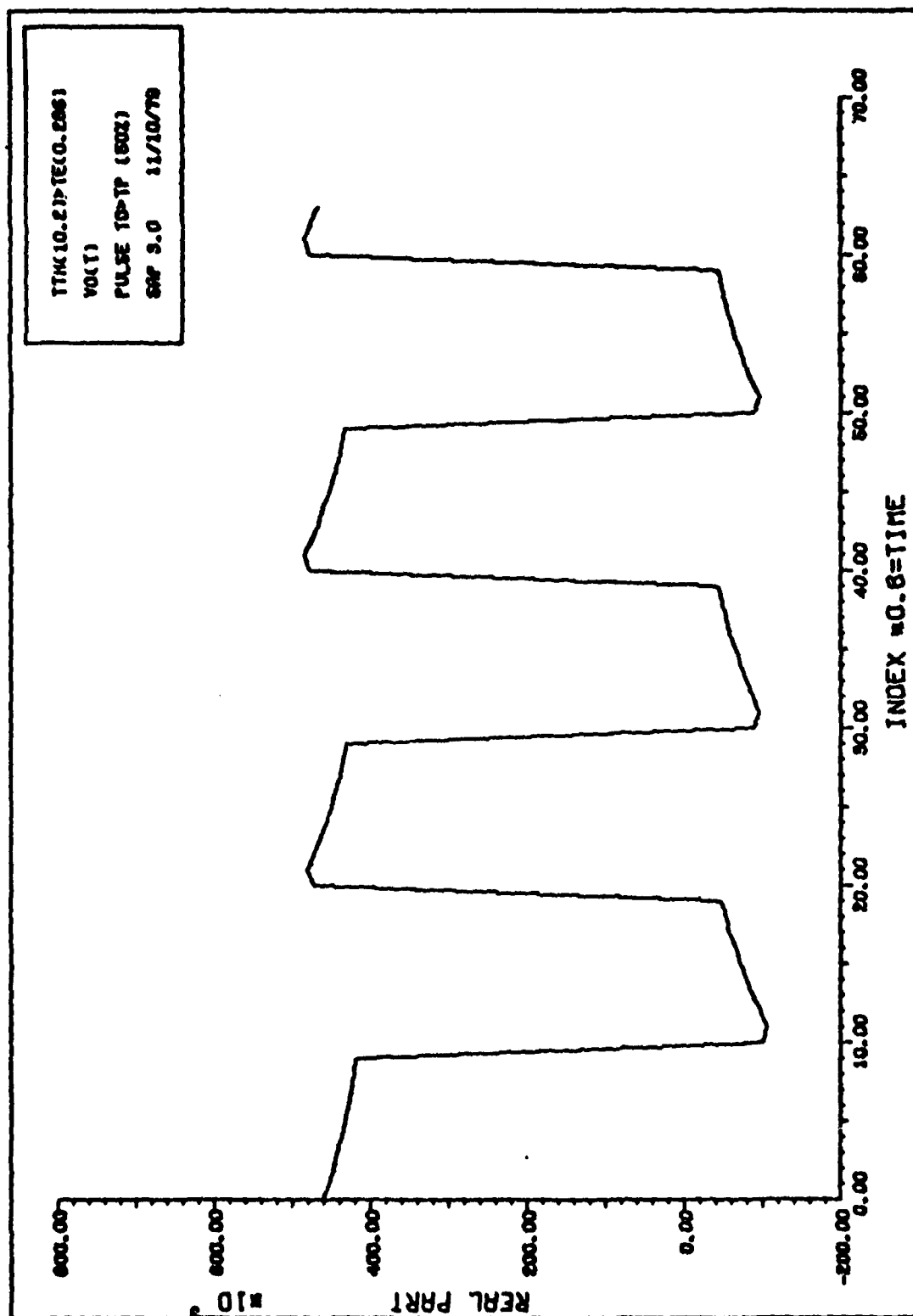


Figure 10. Pyroelectric Sensor Output Voltage due to a Pulse Train

and electrical time constants determined by the material properties and preamplifier load, respectively. The linear properties of the sensor are therefore dependent upon the large detector resistance which is approximately constant over frequency.

When operating the detector with a voltage mode preamplifier the load resistance value greatly affects the detector response. For $R = R_d$ (very large) the electrical bandwidth is narrow and ranges over frequencies less than $1/T_{TH}$. However, for $R \ll R_d$, the bandwidth is broader over frequencies greater than $1/T_{TH}$. The current mode of operation assumes a small feedback capacitance which is very small with respect to open loop amplifier gain and an effective load resistance much less than R_d . Therefore, the current mode is associated as a broad band detector which can similarly be stated as providing fast detection.

For signal detection of pulses with a small pulse width it would be desirable to operate the detector in the current mode. For output signals resembling the incident radiation the pulse widths must be greater than the time for the signal to reach its maximum peak value. The detector can be operated in both voltage and current modes for modulating frequencies greater than the reciprocal of the thermal time constant. However, for frequencies less than the thermal response frequency the detector must have an equivalent load resistance approximately equal to the detector resistance.

IV. Detector Noise Model

The noise expected from the different sources in a pyroelectric point detector are described by a composite noise circuit, by relating the noise power density to an ensemble average noise current. Expressions are presented for the following noise sources: (1) temperature-fluctuation noise from the detector, (2) dielectric loss tangent noise from the detector, (3) preamplifier thermal load noise, (4) preamplifier gate current noise, and (5) preamplifier noise voltage.

The practical pyroelectric detector transducers not only radiation but also noise. In an ideal case, there is no other loss of heat except the radiation, and the noise present is due to the temperature-fluctuation of the incident radiation. In practice, the transduction of radiation into an electrical signal is not ideal, and the electrical response needs amplification to be useful. The performance of practical pyroelectric detectors is thus degraded from the ideal detector because of the transducer efficiency, and the additional noise sources resulting from the dielectric loss of the pyroelectric and load resistance of the preamplifier. Analyzing each noise source generated by the sensor, a composite noise circuit can be obtained. It is assumed that each noise source is generated independently of the others.

Detector Noise Sources

Temperature-Fluctuation Noise. The theoretical limiting noise in an ideal pyroelectric detector is temperature-fluctuation noise (Ref 34: 11-28). Consider the pyroelectric detector as a small black-body receiving radiation, the radiation gives rise to a temperature increase ΔT of the black-body. The differential equation of the system

(Ref 27:212)

$$C^E b A \frac{\partial \Delta T}{\partial t} + g_R A \Delta T = \phi(t) \quad (30)$$

where $\phi(t)$ is the random fluctuation in power exchanged between the detector and its surroundings, with a mean-square fluctuation given by

$$\overline{\phi(t)^2} = 4kT^2 g_R A \Delta f, W^2 \quad (31)$$

where $(\overline{})$ denotes ensemble average. The spectral density (Ref 29:409) is given by

$$S_{\phi}(f) = 4kT^2 g_R A \frac{(\text{Joule})^2}{\text{sec}} \quad (32)$$

which is constant over all frequencies, f , of interest (White noise), and therefore the corresponding input noise current source has a spectral density given by

$$S_{i_T}(f) = 4kT^2 g_R A |R_i(f)|^2 = \frac{4kT^2 A (2\pi f)^2 \eta^2 \lambda^2}{g_R (1 + (2\pi f T_{TH})^2)} (\text{Amp})^2 \text{sec} \quad (33)$$

The average noise current is given by $\sqrt{i_T^2} = \sqrt{\int_{-\infty}^{\infty} S_{i_T}(f) df}$, and the spectral density is plotted in Figure 11. For the case when $2\pi f \ll \frac{1}{T_{TH}}$, $S_{i_T}(f) = \frac{4kT^2 (2\pi f)^2 \eta^2 \lambda^2 A}{g_R 4kT^2 g_R A \eta^2 \lambda^2} = 5.14 \times 10^{-30} f^2 \text{ Amp}^2 \text{sec}$, and when $2\pi f \gg \frac{1}{T_{TH}}$, $S_{i_T}(f) = \frac{4kT^2 A (2\pi f)^2 \eta^2 \lambda^2}{C^E b)^2} \approx 1 \times 10^{-33} (\text{Amp})^2 \text{sec}$. It is apparent that the sensor unit acts a linear filter coloring the white noise at low frequencies ($2\pi f \ll 1/T_{TH}$).

Dielectric Loss Noise. The thermal noise of the detector itself can be described by the Johnson-Nyquist relation where the noise is attributed to the velocity fluctuations of the electrons (charge carriers) in the device resistance R_d . If the detector has a capacitance C_d and a dielectric loss factor $\tan \delta$, and the loss conductance, $g_d = 2\pi f C_d \tan \delta$, then the noise source has a spectral density (Ref 31:590).

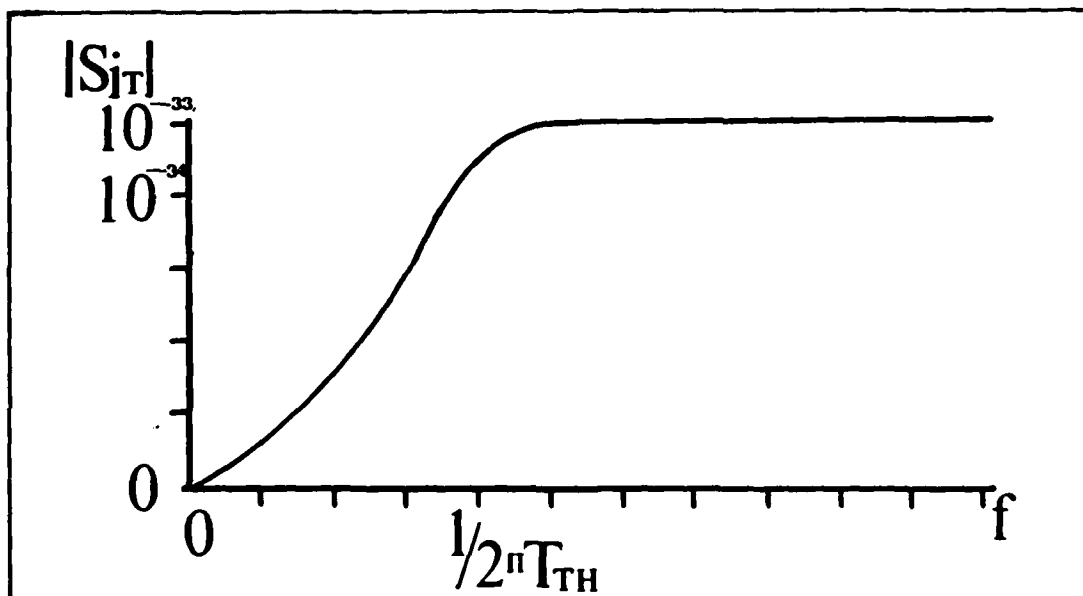


Figure 11. Temperature-Fluctuation Noise Power Spectral Density

$$S_{id}(f) = 4kT g_d = 4kT 2\pi f C_d \tan\delta \quad (\text{Amp})^2 \text{sec} \quad (34)$$

The noise spectral density is consistent with the Johnson-Nyquist noise definition (Ref 36:469), however, for $\tan\delta \approx \text{constant}$ it is inconsistent with the power spectral density definition that $S_{id}(f) \geq 0$ for all frequencies (Ref 17:338). When the pyroelectric material has a low intrinsic dielectric loss, the dielectric loss tangent is given by equation 11 (see also Appendix A). Therefore, substituting equation 11 into equation 32, the noise spectral density becomes

$$S_{id}(f) = \frac{4kT^2 (2\pi f)^2 A \lambda^2}{g_R (1 + (2\pi f T_{TH})^2)} \quad (\text{Amp})^2 \text{sec} \quad (35)$$

It is apparent that the temperature-fluctuation noise and dielectric loss noise are equivalent for low intrinsic dielectric loss materials.

Amplifier Noise Sources

Load Thermal Noise. The amplifier circuit described for both the current and voltage modes in chapter three consisted of an external resistance connected across the detector electrodes. The noise current generated by the random motion of charge carriers within the resistance has a spectral density (Ref 36:469-70) given by

$$S_{iL} = \frac{4kT}{R_L} \quad (\text{Amp})^2\text{sec} \quad (36)$$

and is described by $\sqrt{i_L^2}$. For a load resistance of $8 \times 10^5 \Omega$, $S_{iL} = 1.07 \times 10^{-26} \text{ Amp}^2\text{sec}$.

Gate Current Noise. At the input of both the junction FET amplifier stage and the operational amplifier, there is an additional noise source. Two d.c. currents, I_{g1} and I_{g2} , flow across the gate junction giving full-shot noise (Ref 33:54) so that the noise spectral density is given by

$$S_{ig} = 2e (I_{g1} + I_{g2}) \quad (\text{Amp})^2\text{sec} \quad (37)$$

where e is the electron charge. When I_{g1} and I_{g2} are equal and opposite one another the sum becomes $2I_{go}$. Therefore, the spectral density becomes

$$S_{ig} = 4e I_{go} \quad (\text{Amp})^2\text{sec} \quad (38)$$

Typically, the gate current is approximately 10^{-17} amp such that $S_{ig} \approx 6.4 \times 10^{-36} \text{ Amp}^2\text{sec}$.

Amplifier Noise Voltage. If the amplifier has an equivalent noise resistance, R_n , then the amplifier noise at the output has a spectral density (Ref 31: 591)

$$S_{vn} = 4kT R_n \quad (\text{Volts})^2\text{sec} \quad (39)$$

For an FET, R_n is typically $10^4 \Omega$, and $S_{vn} \approx 1.65 \times 10^{-16} \text{ (Volts)}^2 \text{sec}$.

Noise Equivalent Circuit

The equivalent circuit of the sensor unit including the noise sources is shown in Figure 12 (Ref 15:18) where C_e is the preamplifier equivalent capacitance, and the noise current sources are as described previously. The rms (average) noise currents and noise voltage are obtained by integrating the noise power spectral density over a frequency bandwidth B extending from $-\infty$ to ∞ .

Assuming the noise sources are independent of one another, the total noise power spectrum is given as

$$S_v(f) = (S_{iT}(f) + S_{id}(f) + S_{iL} + S_{ig}) |H(f)|^2 + S_{vn} \quad (40)$$

where $H(f) = R_e / (1 + j2\pi f T_e)$, $R_e = R_d || R_l$, and $T_e = R_l (C_d + C)$. Substituting equations 33, 35, 36, 38, and 39 into equation 40 yields

$$S_v(f) = \left(\frac{8kT^2(2\pi f)^2 A \lambda^2}{g_R(1 + (2\pi f T_{TH})^2)} + \frac{4kT}{R_e} + 4e I_{go} \right) \frac{R_e^2}{(1 + (2\pi f T_e)^2)} + 4kT R_n \quad (41)$$

(Volt)²sec

When the detector conductivity g_d in equation 34 is approximated as a constant, the detector and amplifier Johnson noises can be lumped together (Ref 20:264). The limiting noise term becomes the temperature-fluctuation noise and dielectric loss noise. For the range of practical values of R_l , it will always be much less than R_d . Therefore, for $R_l = 8 \times 10^5 \Omega$ and $2\pi f \ll 1/T_e$, the amplifier Johnson noise becomes the dominant noise contribution and for $f > 16 \text{ KHz}$ the voltage amplifier noise is dominant.

Summary

The pyroelectric detector-preamplifier sensor unit has a

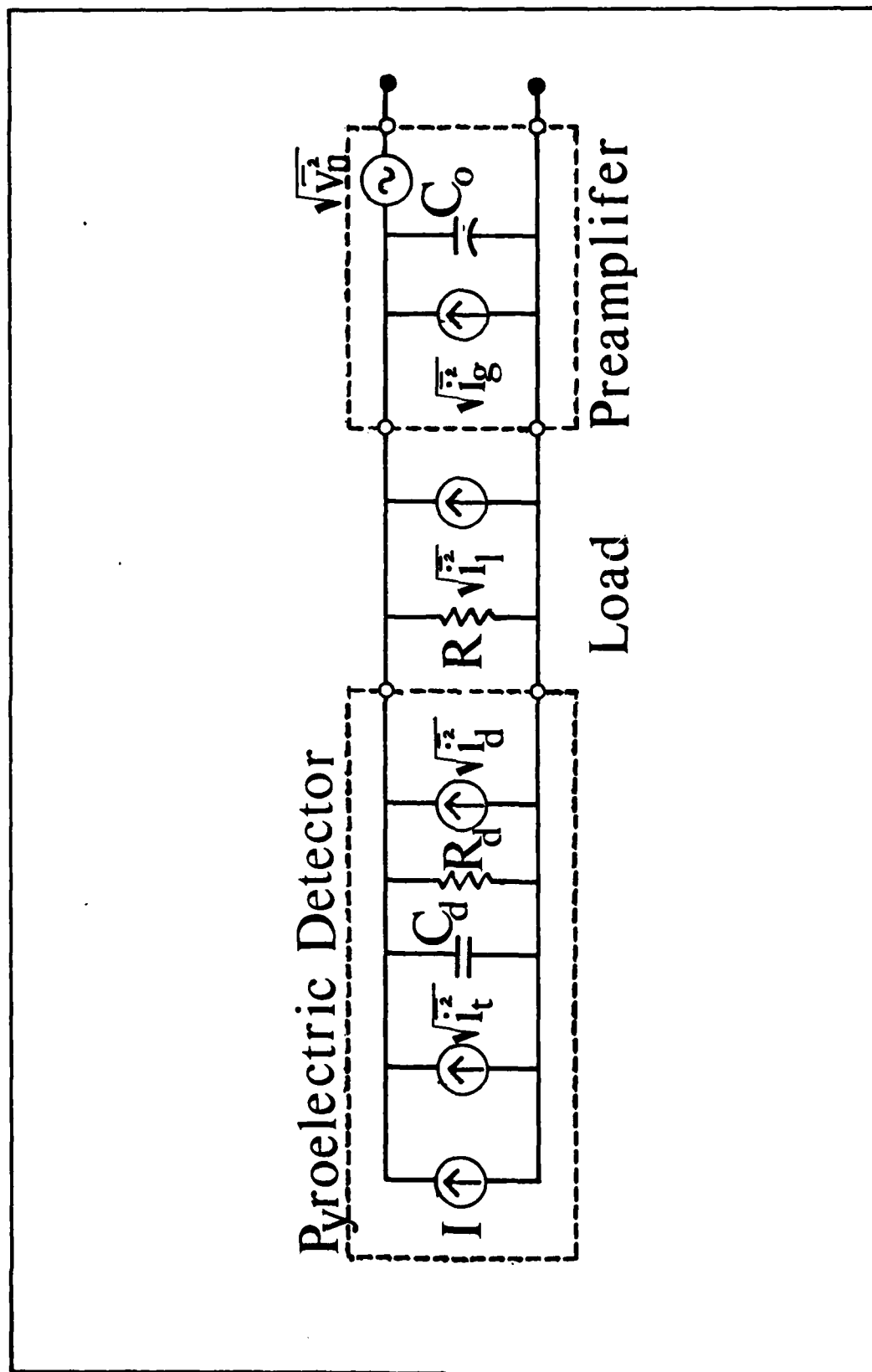


Figure 12. Composite Noise Equivalent Circuit

theoretically limiting noise due to the random fluctuations in the material temperature. However, this theoretical noise limit is not reached since the practical detector is dominated by the thermal noise of the preamplifier resistance. Therefore, the thermal noise generated by the load resistance is considered as the dominant source for frequencies less than $1/2\pi T_e$. The preamplifier network essentially limits the range of the noise power spectrum, and thereby colors the noise source characteristics. The thermal noise influence can be significantly reduced by choice of a large load resistance on the order of the detector resistance. Whether the condition is possible or not depends upon a value for $R_e \geq 10^{11}\Omega$ is practically obtainable.

V. Noise Filtering & Signal Response

By comparison of the average noise power with the average signal magnitude, the detectability of the signal from noise can be determined. Often it is possible to match a filter to the time reverse of the signal waveform in order to maximize the signal-to-noise ratio (SNR) with white noise. The noise may be filtered in such a manner as to frequency compensate the effect of the sensor band limiting effect upon the noise so as to flatten the noise spectrum over all frequencies. This filtering is called whitening such that the resultant noise power spectrum is constant over a practical range of frequencies.

The SNR provides the necessary information to determine which parameters influence the signal power the most when compared with the noise power. The SNR is defined as the ratio of the average instantaneous peak signal to the average noise such that

$$\text{SNR} = \frac{V(t)^2}{\sigma_n(t)^2} = \frac{\left| \int_{-\infty}^{\infty} V(f) e^{j2\pi ft} df \right|^2}{\int_{-\infty}^{\infty} S_v(f) df} \quad (42)$$

where $V(f)$ and $S_v(f)$ were defined by equations 27 and 41, respectively.

The SNR at the output of the matched filter, sampled at the signal peak, is compared to the SNR at the sensor output. The ratio of the SNR's can be used to show the effect of the filter network upon the signal processing.

Pyroelectric Detector Sensor Unit SNR

With the dominant Johnson noise the noise power spectrum given by equation 42 reduces to

$$S_{v_L}(f) = \frac{4kT}{R_L} \frac{R_e^2}{(1 + (2\pi f T_e)^2)} \quad (43)$$

The SNR for the sensor unit shown in Figure 12 is obtained by substituting equation 21 and equation 43 into equation 42. For a pulse of amplitude F_0 and width t_0 the SNR sampled at time t_0 is given as

$$SNR_1 = \frac{F_0^2 \eta^2 \lambda^2 R_L (T_{TH} T_e)^2 (e^{-t_0/T_{TH}} - e^{-t_0/T_e})^2}{(C^E_b)^2 2kT R_e C_d (T_{TH} - T_e)^2} \quad (44)$$

where voltage gain is unity.

A typical example of the magnitude of the SNR can be obtained using the values in Table I, and $t_0 = 1 \times 10^{-3}$ sec. For $T_{TH} > T_e$, the $SNR_1 = F_0^2 6.032 \times 10^{16}$ and for $T_e > T_{TH}$, the $SNR_1 = F_0^2 4.288 \times 10^{20}$.

Noise Filter Network

The noise with the power spectral density given in equation 43 is a nonwhite noise, which can be whitened by applying a frequency compensation filter (whitening filter, $H_w(f)$) (Ref 35:490). The non-white noise is assumed to be a zero-mean Gaussian noise. The sensor output signal is distorted when passing through the whitening filter, however, with white noise the optimum detection of the signal from white noise can be achieved with a matched filter, $H_m(f)$, (Ref 35) used to maximize the SNR at the filter output. A block diagram of the Optical Receiver including the filter network is shown in Figure 13.

Whitening Filter. Since equation 43 satisfies the Paley-Wiener condition (Ref 35:489) (the linear increase in frequency of the filter must have an upper bound), there exists a linear filter with a transfer function $H_w(f)$, which has a realizable inverse and for which

$$|H_w(f)|^2 = \frac{N_0}{2} \frac{1}{S_v(f)} \quad (45)$$

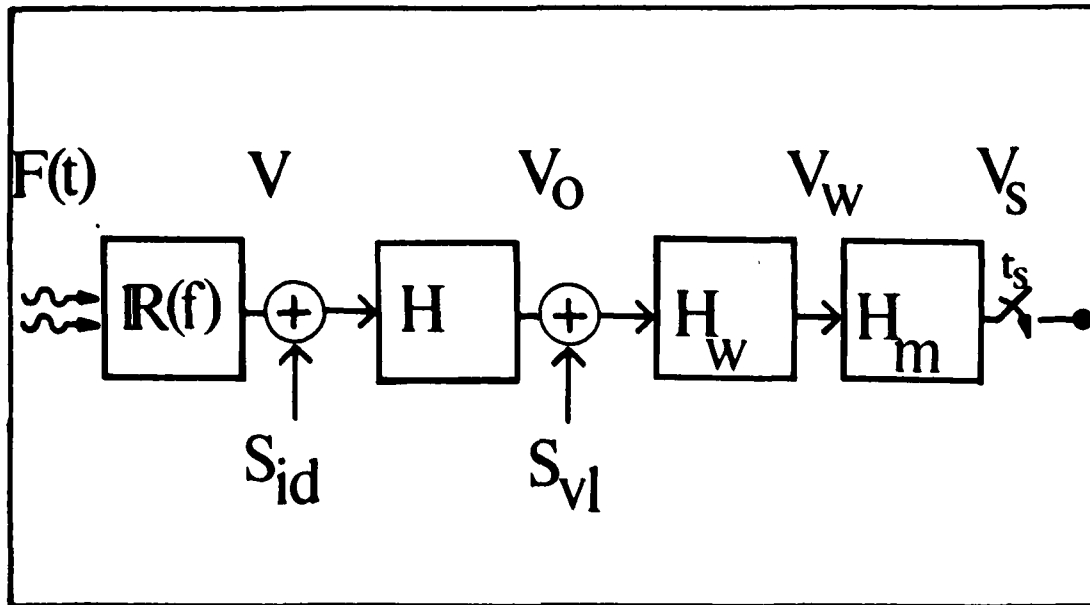


Figure 13. Block Diagram of the Optical Receiver

The $N_o/2$ term is defined as the power spectrum for a stationary, zero-mean Gaussian noise process (Ref 35:189). The filter $H_w(f)$ is called a whitening filter and described by

$$H_w(f) = \frac{1}{2R_e} \frac{RN_o}{2kT} (1 + j2\pi f T_e) \quad (46)$$

The transfer response of cascading the whitening filter and the sensor unit together is given as

$$IR(f) = \frac{V_o(f)H_w(f)}{F(f)} = \frac{j2\pi f \eta \lambda a_v T_e}{C^E C_d b (j2\pi f + 1/T_{TH})2R_e} \frac{R_L N_o}{2kT} \quad (47)$$

For a pulse of width t_o and amplitude F_o , the output signal voltage is given by

$$V_w(t) = \frac{F_o \eta \lambda a_v}{C^E 2b} \frac{R_L N_o}{2kt} (e^{-t_o/T_{TH}} U(t) - e^{-(t-t_o)/T_{TH}} U(t-t_o)) \quad (48)$$

The noise power spectrum (Ref 17:350) is given as

$$S_V(f) = S_{V_L}(f) |H_w(f)|^2 = \frac{N_o}{2}, \quad (49)$$

therefore, substituting into equation 42, the SNR becomes

$$\text{SNR}_2 = \left(\frac{F_o a_v \eta \lambda}{2C^E b} e^{-t_o/T_{TH}} \right)^2 \frac{R_l}{RTB} \quad (50)$$

where in the limit as B the frequency bandwidth goes to infinity, the SNR_2 goes to zero.

Matched Filter. A filter whose impulse response is a delayed, time-reversed version of $V_w(t)$ (equation 48) is called a matched filter, matched to the signal portion of $V_w(t)$ (Ref 30:311). Since the noise from the whitening filter has a power density $N_o/2$ it is possible to obtain an output from a matched filter $V_s(t_s)$ that is considerably greater when a pulse is incident upon the detector than when $F'(t) = 0$. Therefore, the filter makes the instantaneous power in $V_s(t_s)$ as large as possible compared to the average power in the noise at time t_s . In Figure 13, $H_m(f)$ is the transfer function of the matched filter with its output sampled at time t_s , given as

$$H_m(f) = K V_w^*(f) e^{-j2\pi f t_s} \quad (51)$$

where $*$ denotes the complex conjugate. The impulse response of the matched filter for a rectangular pulse signal is given as

$$h_m(t) = \frac{K F_o a_v \eta \lambda}{2C^E b} \frac{R_l N_o}{2kT} (e^{(t-t_s)/T_{TH}} U(t) - e^{(t-t_s+t_o)/T_{TH}} U(t+t_o)) \quad (52)$$

where K is a scaling factor introduced by $H_m(f)$. For the receiver network, the output signal may be obtained by multiplication of the frequency domain representation of $F(t)$ by the product of the responsivity and filter transfer function of the receiver.

Filter Output

For the receiver network shown in Figure 13, the output voltage $V_s(t_s)$ due to an input $F(t) = F_o(U(t) - U(t - t_o))$, is given by

$$V_s(t_s) = K \left(\frac{F_o a_v \eta \lambda}{2} \right)^2 \frac{R_L N_o}{C^E b k T g_R} \left\{ e^{-|t-t_s|/T_{TH}} - \frac{e^{-|t-t_s+t_o|/T_{TH}} - e^{-|t-t_s-t_o|/T_{TH}}}{2} \right\} \quad (53)$$

which was obtained from the inverse fourier transform of (Ref 17:340)

$$V_s(f) = K \left(\frac{F_o a_v \eta \lambda}{2} \right)^2 \frac{R_L N_o}{C^E b k T g_R} \frac{(1 - \cos 2\pi f t_o)}{((2\pi f)^2 + 1/T_{TH}^2)} e^{-j2\pi f t_s} \quad (54)$$

It is possible to obtain the energy of the output signal by applying Parseval's Theorem (Ref 36:35) to equation 53.

The sampling time t_s is chosen when the signal peak is maximum.

The SNR is therefore maximum when Ref (36:312)

$$SNR_3 = \frac{2}{N_o} \int_{-\infty}^{\infty} |V_o(f) H_w(f)|^2 df \quad (55)$$

which becomes (Ref 11:447),

$$SNR_3 = \left(\frac{F_o a_v \eta \lambda}{2} \right)^2 \frac{R_L 2\pi}{C^E b k T g_R} (1 - e^{-2\pi t_o/T_{TH}}) \quad (56)$$

For the case when $T_e > T_{TH}$, $R \approx 10^{12} \Omega$, $a_v = 10^3$, and $SNR_3 = F_o^2 9.808 \times 10^{25}$ then $SNR_3/SNR_1 = 2.28 \times 10^5$. For the case when $T_{TH} > T_e$, $R \approx 10^9 \Omega$, $a_v = 10^3$, and $SNR_3 = F_o^2 9.808 \times 10^{22}$ then $SNR_3/SNR_1 = 1.62 \times 10^6$. Therefore, an improvement in SNR is possible with the cascaded filtering network, and between detector modes of operation there is a difference of 10.

Summary

The thermal noise generated by the load resistance is colored by the preamplifier network. The colored noise spectrum dominates over the signal spectrum at frequencies less than $1/T_e$. The signal-to-noise ratio can be improved by a factor of 10^6 with a cascaded network of whitening filter and matched filter connected with the sensor unit. The combination of cascaded filter network and sensor unit comprise the optical receiver. The signal detection is optimized when the matched filter has a transfer response given by equation 52.

VI. Conclusion

From the list of thermal detectors known to date, the pyroelectric detector is a promising addition to useful detectors. The pyroelectric nature of the crystalline material is determined by its unique properties, of noncentrosymmetry and single coefficient of pyroelectricity, to produce a current signal due to changes in the material temperature. The pyroelectric transduces not only IR radiation but also noise signals which are detectable at the sensor output. The responsivity of the detector can be described to produce either a current or a voltage due to the capacitive nature of the pyroelectric.

The detector signal output can be monitored by applying either a current or voltage mode preamplifier network. The choice of the load resistance of the preamplifier is used to determine the frequency bandwidth of the sensor response. For the current mode it is possible that the bandwidth will be broad for a resistance much less than the detector resistance, and extends for frequencies greater than the thermal response frequency. However, for the voltage mode the sensor has a narrow band frequency response for very large load resistances at frequencies less than the thermal response frequency and a broadband response for small resistances similar to the current mode.

No matter in what mode the detector is operated the output voltage is modeled by the same equation. The desirable operating constraint is that incident pulse width be greater than the time for the detector to reach a maximum output.

Thermally generated noise from the load resistance dominates the noise power spectrum for values of $R_e > R_n$ and $f < 1/2\pi T_e$. Thermally generated noise within the detector is described by the dielectric

nature of the pyroelectric and called dielectric loss noise. It can be shown that the dielectric loss noise, for a low intrinsic dielectric loss material, is on the order of the theoretically limiting noise due to temperature-fluctuations.

Since the nonwhite thermal noise from the sensor dominates the noise spectrum, a small equivalent load resistance is desired. The constraint limits the detector operation to the broad-band configuration. It is, therefore, possible to detect narrow pulse widths for modulation frequencies greater than the thermal response frequency. With frequency compensation of the noise spectral density the noise is whitened. The detector signal may then be optimally detected by a matched filter.

Further work necessary upon the detector design will consist of a description of the uniformity between pyroelectrics such that their use in detector arrays may be possible. It was noted that such work is in progress, however, much remains to be determined.

Bibliography

1. Blevin, W. R. and Jon Geist. "Influence of Black Coatings on Pyroelectric Detectors," Applied Optics, 13: 1171-1178 (May 1974).
2. Burdick, Glenn A. and Roy J. Arnold. "Theoretical Expressions for the Noise Equivalent Power of Pyroelectric Detectors," Journal of Applied Physics, 37: 3223-3226 (July 1966).
3. Burfoot, Jack C. Ferroelectrics; An Introduction to the Physical Principles. London: D. Van Nostrand Company LTD., 1967.
4. Cady, Walter Guyton. "Piezoelectricity," 1 and 2. New York: Dover Publications, Inc., 1964.
5. Carslaw, H.S. and J. C. Jaeger. Conduction of Heat in Solids. London: Oxford University Press, 1959.
6. Cooper, J. "A Fast-Response Pyroelectric Thermal Detector," Journal of Scientific Instruments, 39: 367-472, (1962).
7. Daniel, Vera V. Dielectric Relaxation. New York: Academic Press, 1967.
8. Eng, J. T. and R. A. Gudmundsen. "Theory of Optical Heterodyne Detection Using the Pyroelectric Effect," Applied Optics, 19: 161-166, (January 1970).
9. Frohlich, Herbert. Theory of Dielectrics; Dielectric Constant and Dielectric Loss. London: Oxford University Press, 1967.
10. Geist, Jon and W. R. Blevin. "Chopper-Stabilized Null Radiometer Based Upon an Electrically Calibrated Pyroelectric Detector," Applied Optics, 12: 2532-2535 (November 1973).
11. Gradshtyn, I. S. and I. W. Ryzhik. Table of Integrals, Series, and Products. New York: Academic Press, 1965.
12. Grinich, V. H. and H. G. Jackson. Introduction to Integrated Circuits. New York: McGraw-Hill, 1975.
13. Lang, Sidney, B. "Literature Guide to Pyroelectricity 1974-1975," Ferroelectrics, 14: 807-848, (1976).
14. Levy, Robert A. Principles of Solid State Physics. New York: Academic Press, 1968.
15. Liu, S. T. and Donald Long. "Pyroelectric Detectors and Materials," Proceedings of the IEEE, 66: 14-26, (January 1978).
16. Nye, J. F. Physical Properties of Crystals. London: Oxford University Press, 1957.

17. Papoulis, Athanasios. Probability, Random Variables, and Stochastic Processes. New York: McGraw-Hill Book Co., 1965.
18. Peterson, R. L., et al. "Analysis of Response of Pyroelectric Optical Detectors," Journal of Applied Physics, 45: 3296-3303, (August 1974).
19. Phelan, Robert J. Jr., and A. R. Cook. "Electrically Calibrated Pyroelectric Optical-Radiation Detector," Applied Optics, 12: 2494-2500 (October 1973).
20. Putley, E. H. "The Pyroelectric Detector," Semiconductors and Semimetals, Vol 5. Editors R. K. Willardson and Albert C. Beer. New York: Academic Press, 1970.
21. -----. "The Pyroelectric Detector - An Update," Semiconductors and Semimetals, Vol 12. Edited by R. K. Willardson and Albert C. Beer. New York: Academic Press, 1977.
22. Roundy, Carlos B. "Solid-State Pyroelectric Infrared Image Converter," Infrared Physics, 19: 507-522 (October 1979).
23. Schilling, D. L. and C. Belove. Electronic Circuits: Discrete and Integrated. New York: McGraw-Hill, 1968.
24. Shaulov, A. and M. Simhony. "Pyroelectric Voltage Response to Rectangular Infrared Signals in Triglycine Sulphate and Strontium-Barium Niobate," Journal of Applied Physics, 43: 1440-1444 (April 1972).
25. -----. "Internal Bias Effects on Pyroelectric Measurements Near the Curie Temperature in Triglycine Sulphate," Journal of Applied Physics, 47: 1-5 (January 1976).
26. Simhony, M. and A. Shaulov. "Pyroelectric Voltage Response to Step Signals of Infrared Radiation in Tryglycine Sulphate and Strontium-Barium Niobate," Journal of Applied Physics, 42: 3741-3744 (September 1971).
27. Smith, R. A., F. E. Jones and R. P. Chasmar. The Detection and Measurement of Infrared Radiation, (Second Edition), London: Oxford University Press, 1968.
28. Stokowski, S. E. "Temperature Noise and Dielectric Loss in Pyroelectric Detectors," Applied Physics Letters, 29: 393-395 (October 1976).
29. Vander Ziel, Aldert. Noise. New York: Prentice-Hall, Inc., 1954.
30. -----. Noise: Sources, Characterization, and Measurement. New Jersey: Prentice-Hall, Inc., 1970.
31. Vander Ziel, A., and S. T. Liu. "Noise Sources in Pyroelectric Radiation Detectors," Physica 61: 589-593 (1972).

32. ----. "Diffusion Theory of the Response of Pyroelectric Detectors," Journal of Applied Physics, 43: 4260-4261 (October 1972).
33. Vander Ziel, Aldert. Noise in Measurements. New York: John Wiley and Sons., 1976.
34. Wolfe, William L. and George J. Zissis. Infrared Handbook. Environmental Research Institute of Michigan. Office of Naval Research, Department of the Navy, Washington DC.
35. Wozencraft, J. M. and I. M. Jacobs. Principles of Communication Engineering. New York: John Wiley and Sons Inc., 1965.
36. Ziemer, R. E. and W. H. Tranter. Principles of Communications. Boston: Houghton Mifflin Co., 1976.

Appendix A

Material Conductance & Dielectric Loss Factor

The purpose of this Appendix is to present the relation between the detector loss tangent and the radiative and thermal conductance. The connection can be demonstrated via thermodynamic arguments. The material parameters contributing to the pyroelectric voltage response and the temperature-fluctuation noise are the pyroelectric coefficient, the dielectric constant, and the volume specific heat. The measured values of these parameters, however, depend on whether or not the pyroelectric is free to change its volume and shape. When the crystal is mechanically clamped and restrictions imposed upon change in shape, the secondary pyroelectricity is reduced. The properties of the pyroelectric are therefore described by the electric displacement and the entropy of the crystal.

In a pyroelectric material the coupling between the electrical and thermal properties is described by the following expressions (Ref 16: Ch 10; 28). The electric displacement can be written in differential form as

$$dD_1 = \epsilon_0 (1 + \chi_e) dE_1 + P_s = \epsilon dE_1 + \lambda_1 dT \quad (A-1)$$

where D_1 , E_1 , and λ_1 are electric displacement, electric field, and pyroelectric vector components respectively, ϵ is the dielectric permittivity, χ_e is the susceptibility, T is the material temperature, and P_s is the spontaneous polarization. The differential change in entropy is given by

$$dS = \lambda_1 dE_1 + \left(\frac{C^E}{T}\right) dT \quad (A-2)$$

where S is the entropy and C^E is the heat capacity at constant electric

field (denoted by superscript E) and λ_i is the electrocaloric vector component. For a reversible change of polarization and temperature λ_i in equation A-1 and equation A-2 are the same. Piezoelectric contributions are not included. In order to simplify these equations, assume that the pyroelectric material belongs to one of the eight uniaxial crystals in which the dielectric tensor is diagonal. In this case, there is only one pyroelectric component, which is taken to be λ .

Due to the coupling of the electrical and thermal properties, the measured dielectric function along the polar axis, $\epsilon_x = \epsilon$ (see Figure 1(a)), is dependent upon T. Therefore, equation A-1 gives

$$\frac{dD}{dE} = \epsilon + \lambda \frac{dT}{dE} \quad (A-3)$$

where $\frac{dP_i}{dE_i} = \frac{dP_i}{dT} \frac{dT}{dE_i} = \lambda \frac{dT}{dE}$. The second law of thermodynamics for a reversible change is given by

$$dQ = TdS \quad (A-4)$$

where Q is the amount of heat flow into the crystal. Substitution of equation A-2 into equation A-4 gives

$$dQ = \lambda T dE + C^E dT. \quad (A-5)$$

Given the thermoconductivity G_T , as

$$G_T = -V \frac{d}{dT} \left(\frac{dQ}{dT} \right) \quad (A-6)$$

where V is the volume of the crystal. Substitution of equation A-5 into equation A-6 and taking the Fourier Transform

$$\frac{G_T}{C^2 V} = -j2\pi f \left(\lambda \frac{T}{C^E} \frac{dE}{dT} + 1 \right). \quad (A-7)$$

Solving equation A-7 for $\frac{dT}{dE}$ and substituting into equation A-3 gives,

$$\tilde{\epsilon} = \epsilon - \frac{\lambda^2 T j2\pi f}{C^E (j2\pi f + 1/T_{TH})} \quad (A-8)$$

where $G_T = g_R A$ such that $T_{TH} = C^E V / G_T$. Denoting $\epsilon = \epsilon' - j \epsilon''$, and solving for ϵ'' and ϵ' respectively,

$$\epsilon'' = \frac{\lambda^2 T 2\pi f b}{g_R (1 + (2\pi f T_{TH})^2)} \quad (A-9)$$

$$\epsilon' = \epsilon - \frac{\lambda^2 T (2\pi f)^2 T_{TH}^2}{C^E (1 + (2\pi f T_{TH})^2)} \quad (A-10)$$

Notice that for $2\pi f \gg 1/T_{TH}$, $\epsilon' \approx \epsilon$ and $\epsilon'' \approx (\lambda/C^E)^2 (T g_R / 2\pi f b)$.

The electrical conductivity, which represents the losses, $\sigma_e = 2\pi f \epsilon''$ can, therefore, be obtained and the conductance of a lossy material given as

$$g_d = \frac{\sigma_e A}{b} = \frac{\lambda^2 T (2\pi f)^2 A}{g_R (1 + (2\pi f T_{TH})^2)} \quad \frac{1}{\Omega} \quad (A-11)$$

For $2\pi f \gg 1/T_{TH}$, $g_d = \lambda^2 T A / g_R T_{TH}^2$ and for $T_{TH} = 10.2$ sec then $g_d = 7.56 \times 10^{-14} \frac{1}{\Omega}$. Notice that $f \gg 0.0156$ Hz is a required condition for constant material conductance to exist.

Denoting $g_d = 2\pi f C_d \tan \delta$ and solving for the loss tangent, $\tan \delta$ is given as

$$\tan \delta = \frac{\lambda^2 T 2\pi f b}{g_R (1 + (2\pi f T_{TH})^2) \epsilon_R \epsilon_0} \quad (A-12)$$

where ϵ_R is constant and for $f \gg 0.0156$ Hz, $\tan \delta \sim 2.66 \times 10^{-22} \frac{1}{f \epsilon_R}$, also when $f \ll 0.0156$ Hz. Then $\tan \delta \sim 1.39 \times 10^{-4} f \ll 2.178 \times 10^{-6}$.

The above expression exists for materials with a small dielectric constant. The result that the material conductance is constant for frequencies $\gg 1/2\pi T_{TH}$ can be extended to the realm of linear analysis only when the condition is also extended.

Appendix B

Electrical Time Constant

The detector resistance is shown in this Appendix dependent upon frequency due to losses in the material conductance, however, for all frequencies R_d is much larger than the preamplifier load resistance. As a result the electrical time constant of the preamplifier network is independent of R_d .

From Appendix A, the detector resistance is given as

$$R_d = \left(\frac{C_{E_b}}{\lambda}\right)^2 \frac{\left(\frac{1}{T_{TH}} + (2\pi f)^2\right)}{T_{g_R} A (2\pi f)^2} \quad (B-1)$$

For $2\pi f \gg \frac{1}{T_{TH}}$, $R_d = 1.334 \times 10^{13} \Omega$ and for $2\pi f \ll 1/T_{TH}$, $R_d = 3.247 \times 10^9 \frac{1}{f^2} \Omega$. For $T_{TH} = 10.2$ sec, $f \ll 0.0156$ Hz such that $R_d \gg 1.33 \times 10^{13} \Omega$. Therefore, for practical values of R_L ($0 - 10^6 \Omega$), $R_d \gg R_L$. However, for very large values of R_L ($10^{12} \Omega$), $R_L \approx R_d$.

For the network shown in Figure B-1 the input impedance is given as

$$Z = \frac{R R_d / (R_d + R)}{1 + j2\pi f C \left(\frac{R R_d}{R + R_d}\right)} \quad (B-2)$$

and the output voltage is given as

$$V_o(f) = V_i(f) H_V(f) = \frac{V_i(f) j2\pi f C_d R_d R / (R_d + R)}{(1 + j2\pi f (C + C_d) R R_d / (R + R_d))} \quad (B-3)$$

where $T_e = (C + C_d) R L R_d / (R_L + R_d)$ and for $R_d \gg R$, $C_d \gg C$, then

$$T_e = R_L C_d.$$

For the network shown in Figure B-2 the input impedance is given as

$$H_1(f) = \frac{R_d R / (R_d + R)}{1 + j2\pi f (C + C_d) R_d R / (R_d + R)} \quad (B-4)$$

and the output voltage is given by

$$V_o(f) = I(f)H_1(f)$$

(B-5)

where $T_e \approx R_l C_d$ for $R_d \gg R_l$ and $C_d \gg C$.

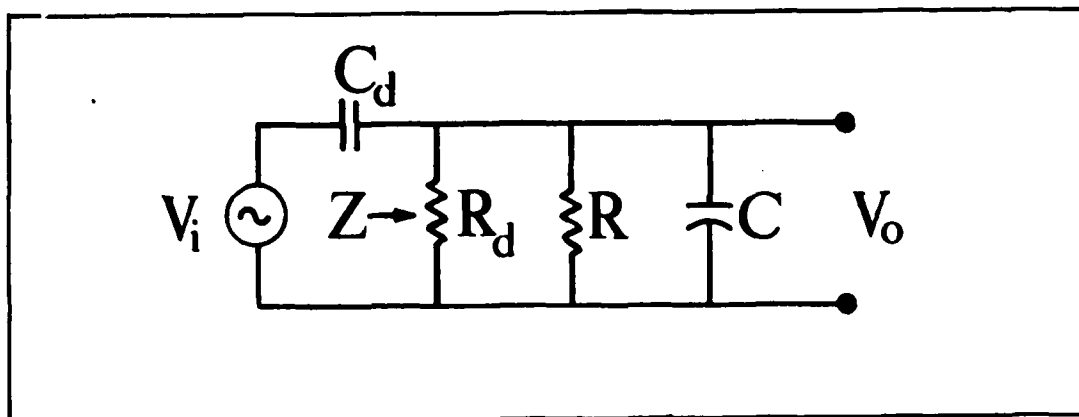


Figure B-1. Voltage Mode R-C Network

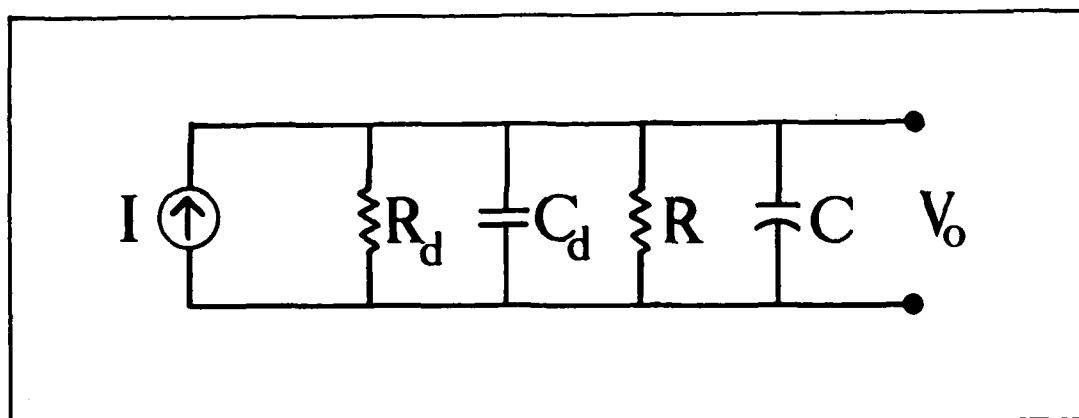


Figure B-2. Current Mode R-C Network

When equation B-1 is substituted into equation B-4, then the electrical time constant is given as

$$T_e = \frac{R_e C_d (1 + (2\pi f T_{TH})^2)}{1 + \gamma^2 (2\pi f T_{TH})^2}$$

where $C_d \gg C$, and $\gamma = \sqrt{\frac{R_l \lambda^2 T_{gR} A}{(C_b)^2} + 1}$. For $R_l \sim 10^5 \Omega$, $\gamma = \sqrt{7.5 \times 10^{-9} + 1} \approx 1$, and $T_e \approx R_l C_d$.

Appendix C

Detector Signal Response

A collection of signal responses from the sensor unit are presented in this appendix for various inputs. The inputs range from a step signal to pulse trains with various duty cycles. The transfer of the pyroelectric sensor unit is given as

$$IR(f) = \frac{j2\pi f \eta \lambda a_v}{C^E C_d b (j2\pi f + 1/T_{TH})(j2\pi f + 1/T_e)}$$

$$IR(t) = \frac{\eta \lambda a_v}{C^E C_d b \left(\frac{1}{T_e} - \frac{1}{T_{TH}}\right)} \left(\frac{1}{T_e} e^{-t/T_e} - \frac{1}{T_{TH}} e^{-t/T_{TH}}\right)$$

for $T_e \gg T_{TH}$

$$IR(t) \approx \frac{\eta \lambda a_v}{C^E C_d b} e^{-t/T_{TH}}$$

for $T_{TH} \gg T_e$

$$IR(t) \approx \frac{\eta \lambda a_v}{C^E C_d b} e^{-t/T_e}$$

The sensor output voltage is given in the frequency domain as

$$V_o(f) = IR(f) F(f) .$$

For the case when $F(t) = 1$ for $t > 0$, then $F(f) = \frac{1}{2} \delta(f) + 1/j2\pi f$,

$$V_o(f) = \frac{\eta \lambda a_v}{C^E C_d b} \left\{ \frac{1}{2} \frac{\delta(f) j2\pi f}{(j2\pi f + 1/T_{TH})(j2\pi f + 1/T_e)} + \frac{1}{(j2\pi f + 1/T_{TH})(j2\pi f + 1/T_e)} \right\}$$

which becomes

$$V_o(f) = \frac{\eta \lambda a_v}{C^E C_d b} \frac{1}{(j2\pi f + 1/T_{TH})(j2\pi f + 1/T_e)}$$

Therefore, the time response is

$$V_O(t) = \frac{\eta \lambda a_v}{C^E C_d b} \frac{1}{\left(\frac{1}{T_e} - \frac{1}{T_{TH}}\right)} (e^{-t/T_{TH}} - e^{-t/T_e})$$

for $T_{TH} \gg T_e$, $V_O(t)$ is plotted in Figure C-1, and for $T_e \gg T_{TH}$,

$V_O(t)$ is plotted in Figure C-2. For the case when $F(t) = \begin{cases} 1 & \text{for } 0 < t < t_0 \\ 0 & \text{else} \end{cases}$

then $F(f) = \frac{1}{j2\pi f} \left\{ 1 - e^{-j2\pi f t_0} \right\}$

$$V_O(f) = \frac{\eta \lambda a_v}{C^E C_d b} \frac{(1 - e^{-j2\pi f t_0})}{(j2\pi f + 1/T_{TH})(j2\pi f + 1/T_e)}$$

therefore, the time response is

$$V_O(t) = \frac{\eta \lambda a_v}{C^E C_d b} \left\{ \frac{(e^{-t/T_{TH}} - e^{-t/T_e}) - (e^{-(t-t_0)/T_{TH}} - e^{-(t-t_0)/T_e})}{\left(\frac{1}{T_e} - \frac{1}{T_{TH}}\right)} \right\}$$

which peaks at $t_p = \frac{T_e T_{TH}}{(T_e - T_{TH})} \ln(T_e/T_{TH})$. Notice that for $T_{TH} \gg T_e$,

$$V_O(t) = \frac{\eta \lambda a_v}{C^E C_d b} \left\{ T_e (1 - e^{-t/T_e}) - T_e (1 - e^{-(t-t_0)/T_e}) \right\}$$

and is plotted for $t_0 > t_p$ in Figure C-3, and for $t_p > t_0$ in Figure C-4.

Notice also that for $T_e \gg T_{TH}$,

$$V_O(t) = \frac{\eta \lambda a_v}{C^E C_d b} \left\{ T_{TH} (1 - e^{-t/T_{TH}}) - T_{TH} (1 - e^{-(t-t_0)/T_{TH}}) \right\}$$

and is plotted for $t_0 > t_p$ in Figure C-5, and for $t_p > t_0$ in Figure C-6.

For the case when $F(t) = \begin{cases} 1 & \text{for } T < t < nT + t_0; n - \text{integer} \\ 0 & \text{else} \end{cases}$ (a pulse train) then

$$F(f) = \frac{1}{j2\pi f} \left\{ \frac{1 - e^{-j2\pi f t_0}}{1 - e^{-j2\pi f T}} \right\}.$$

The output voltage is plotted for $T_{TH} \gg T_e$ when $t_o > t_p$ and the duty cycle of the pulse train is 50% and 95% of the pulse period T in Figures C-7 and C-8, respectively. The output voltage is plotted for $T_e \ll T_{TH}$ when $t_o > t_p$ and the duty cycle of the pulse train is 50%, 75%, and 90% of the pulse period in Figures C-9, C-10, and C-11, respectively.

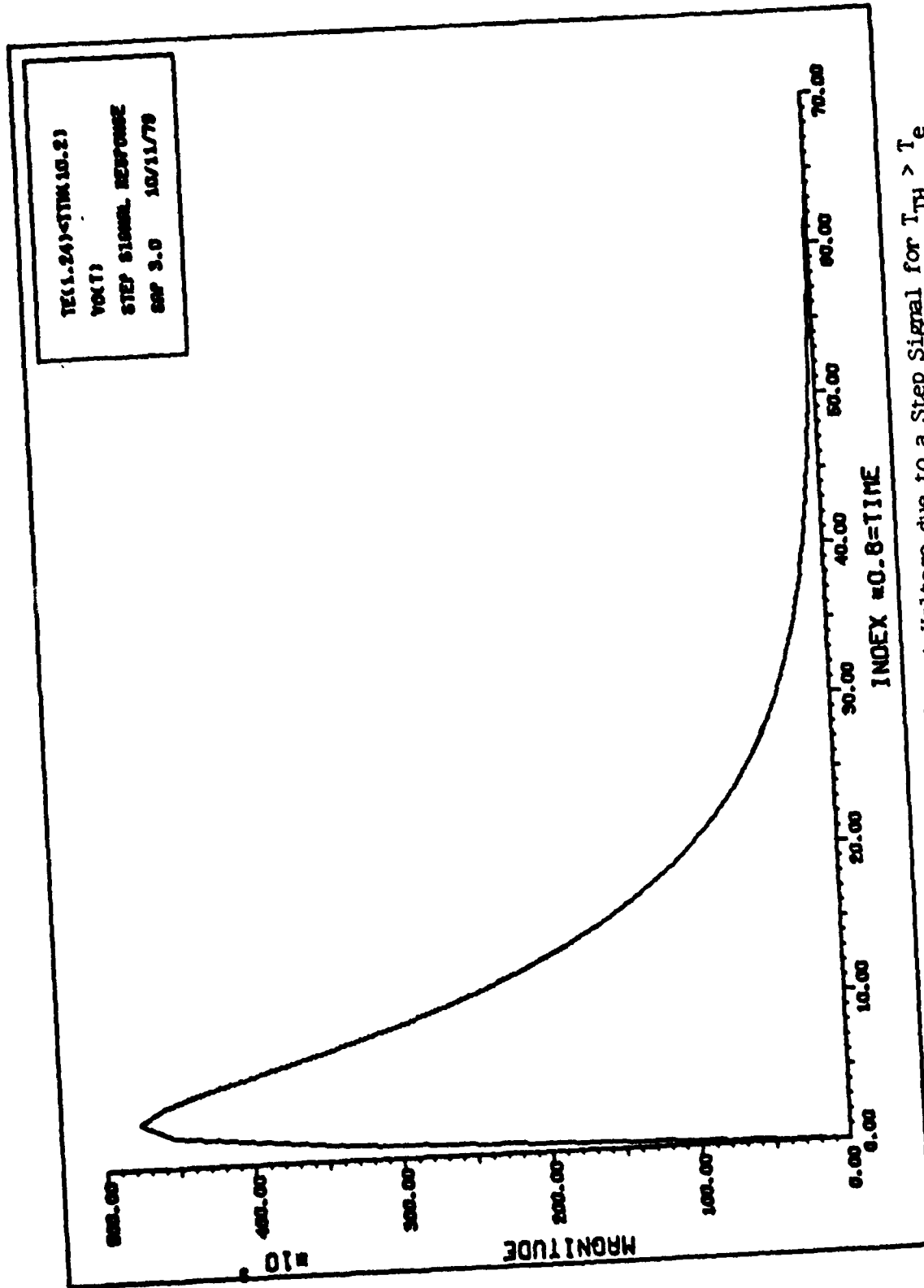


Figure C-1. Pyroelectric Sensor Output Voltage due to a Step Signal for $T_{TH} > T_e$

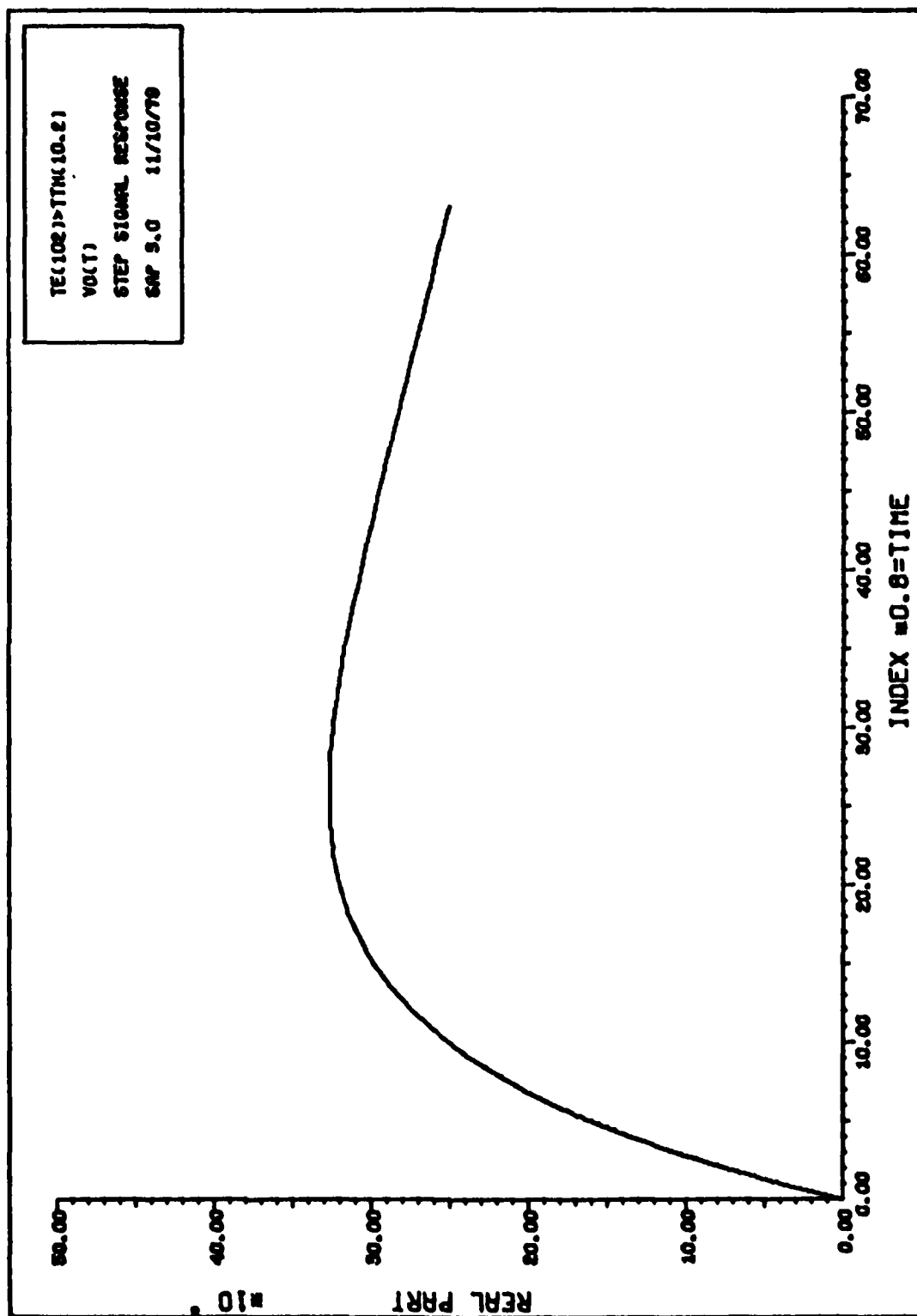


Figure C-2. Pyroelectric Sensor Output Voltage due to a Step Signal for $T_e > T_{TH}$

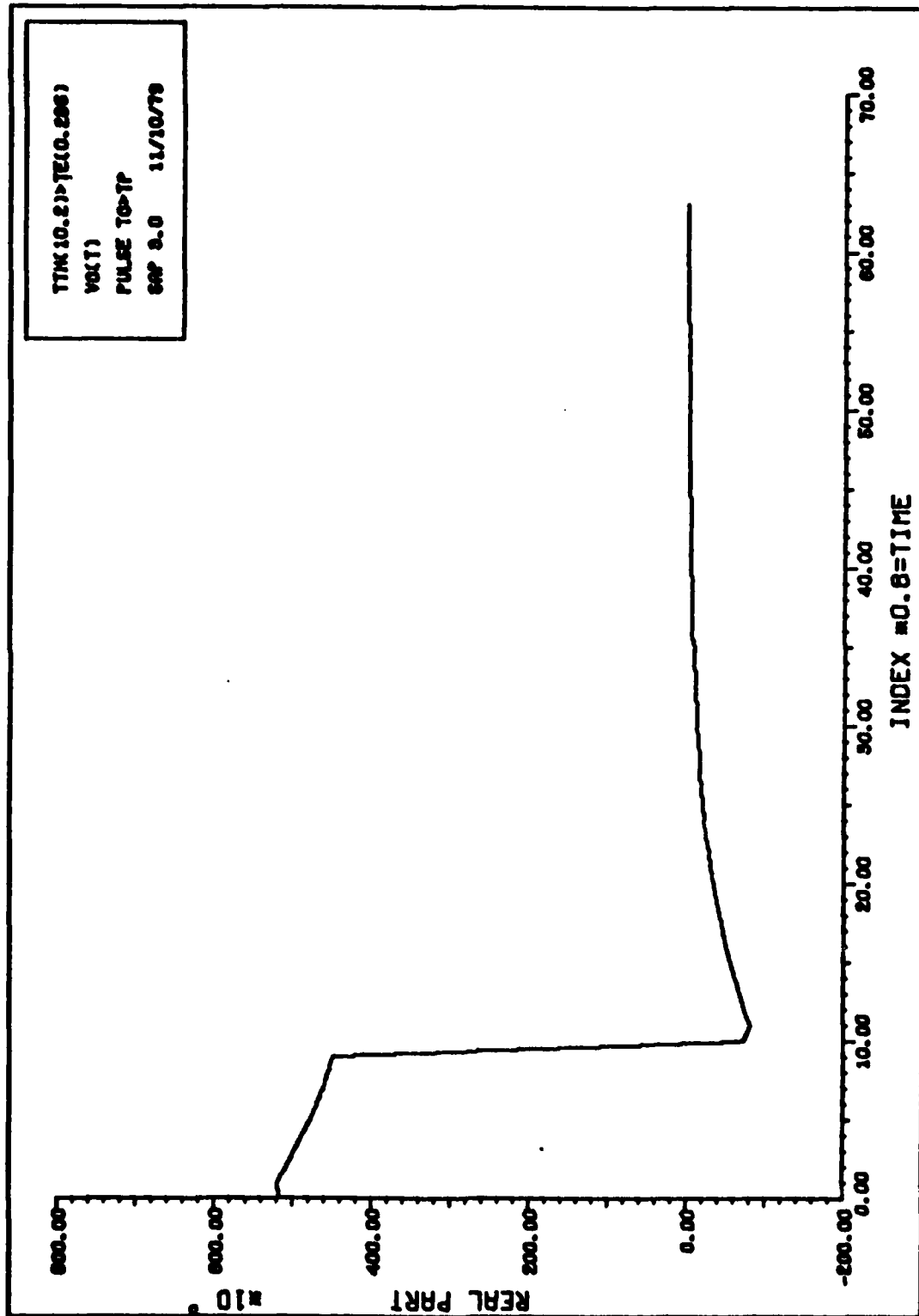


Figure C-3. Pyroelectric Sensor Output Voltage due to a Pulse for $T_{TH} > T_e$ and $t_o > t_p$

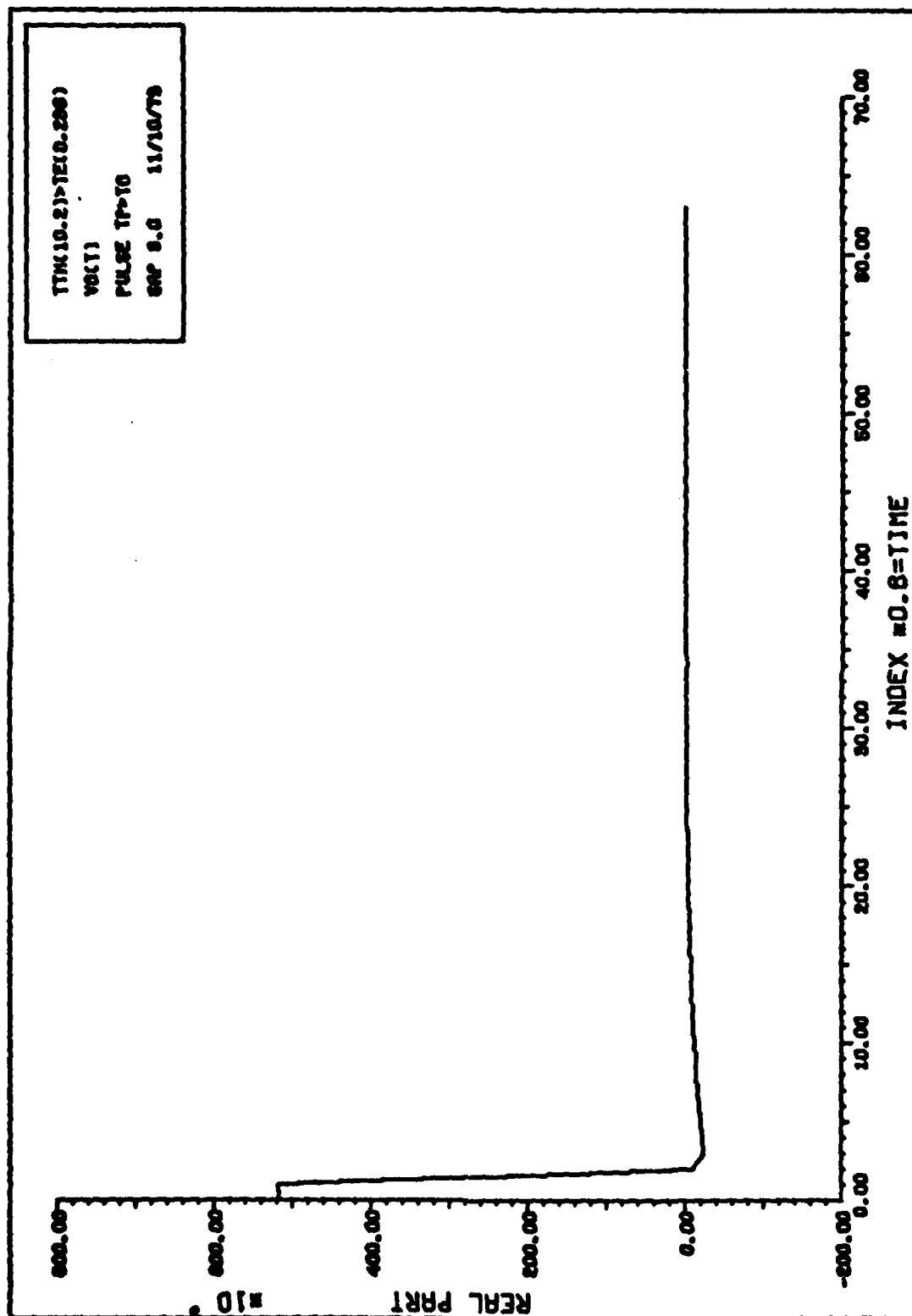


Figure C-4. Pyroelectric Sensor Output Voltage due to a Pulse for $T_{TH} > T_e$ and $t_p > t_0$

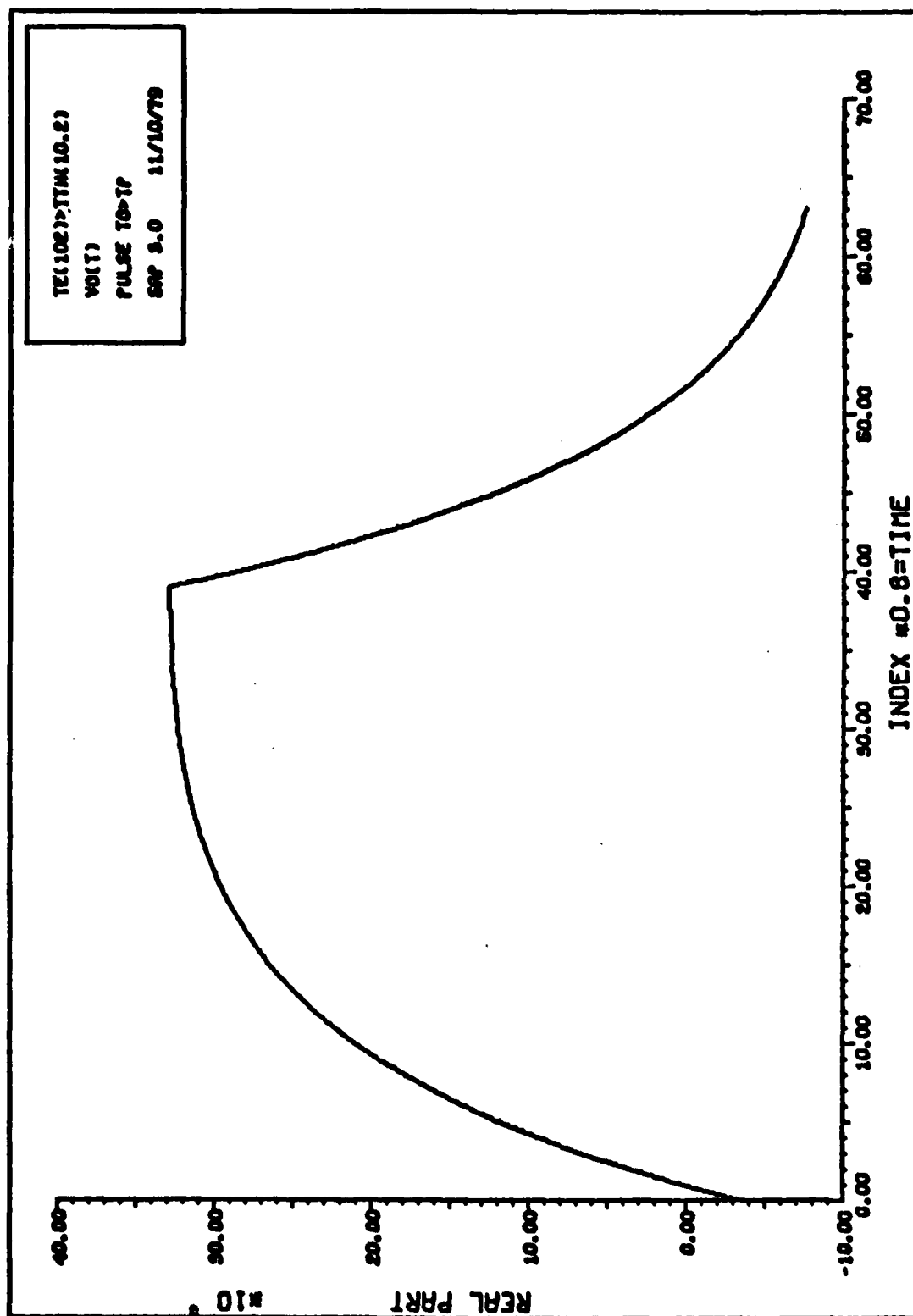


Figure C-5. Pyroelectric Sensor Output Voltage due to a Pulse for $T_e > T_{TH}$ and $t_o > t_p$

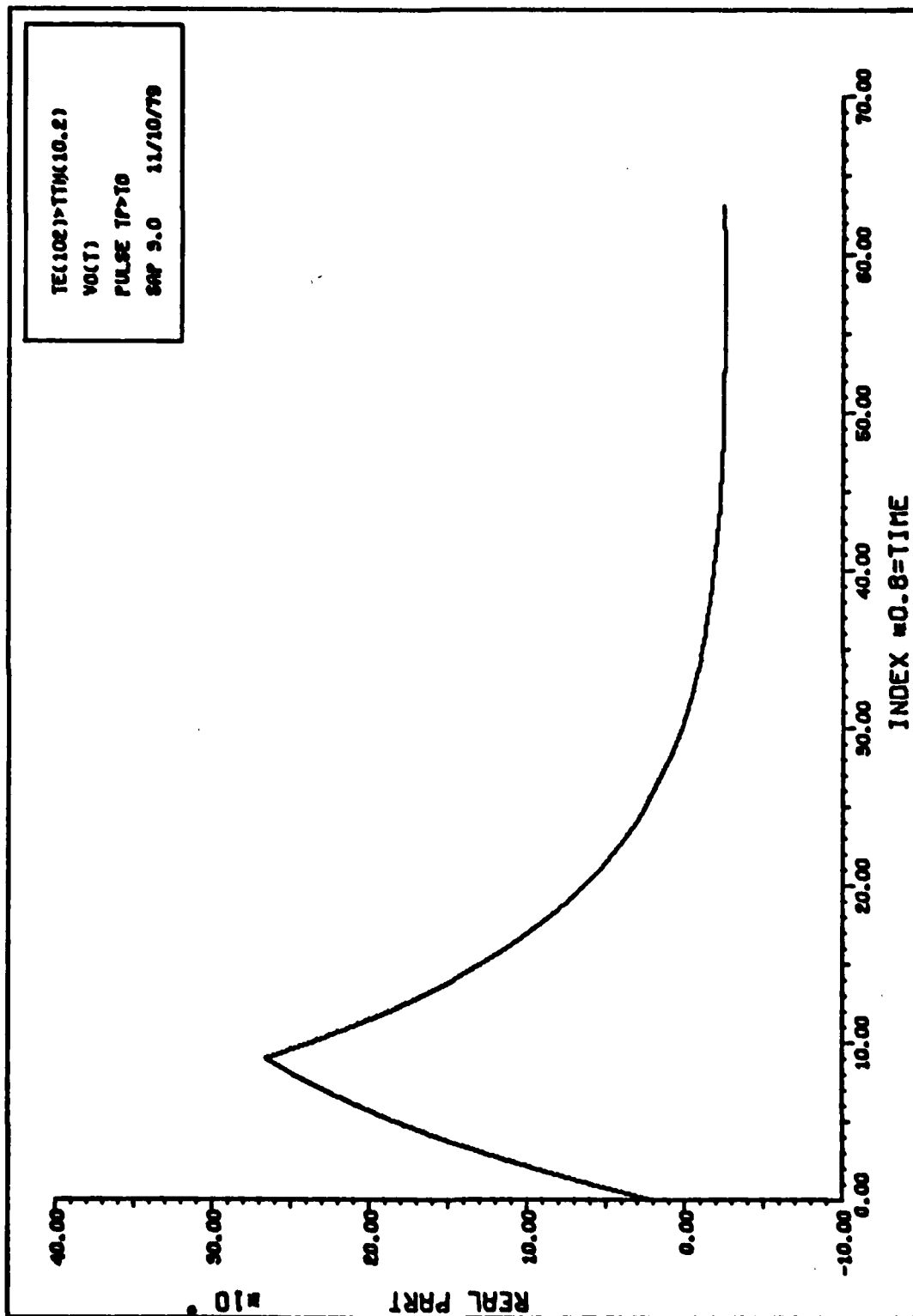


Figure C-6. Pyroelectric Sensor Output Voltage due to a Pulse for $T_e > T_{TH}$ and $t_p > t_o$

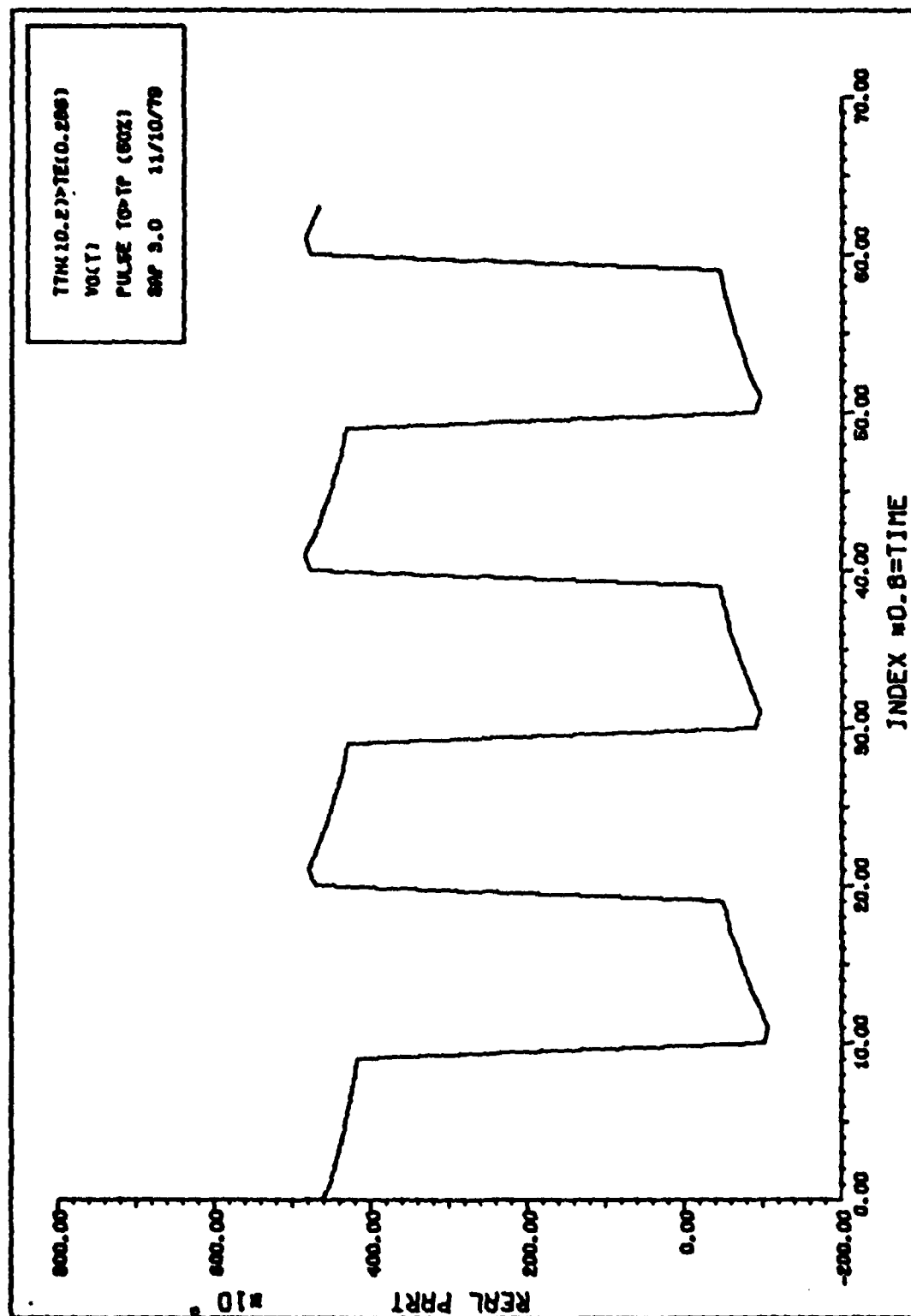


Figure C-7. Pyroelectric Sensor Output Voltage due to a Pulse Train with a 50% duty cycle for $T_{TH} > T_e$ and $t_o > t_p$

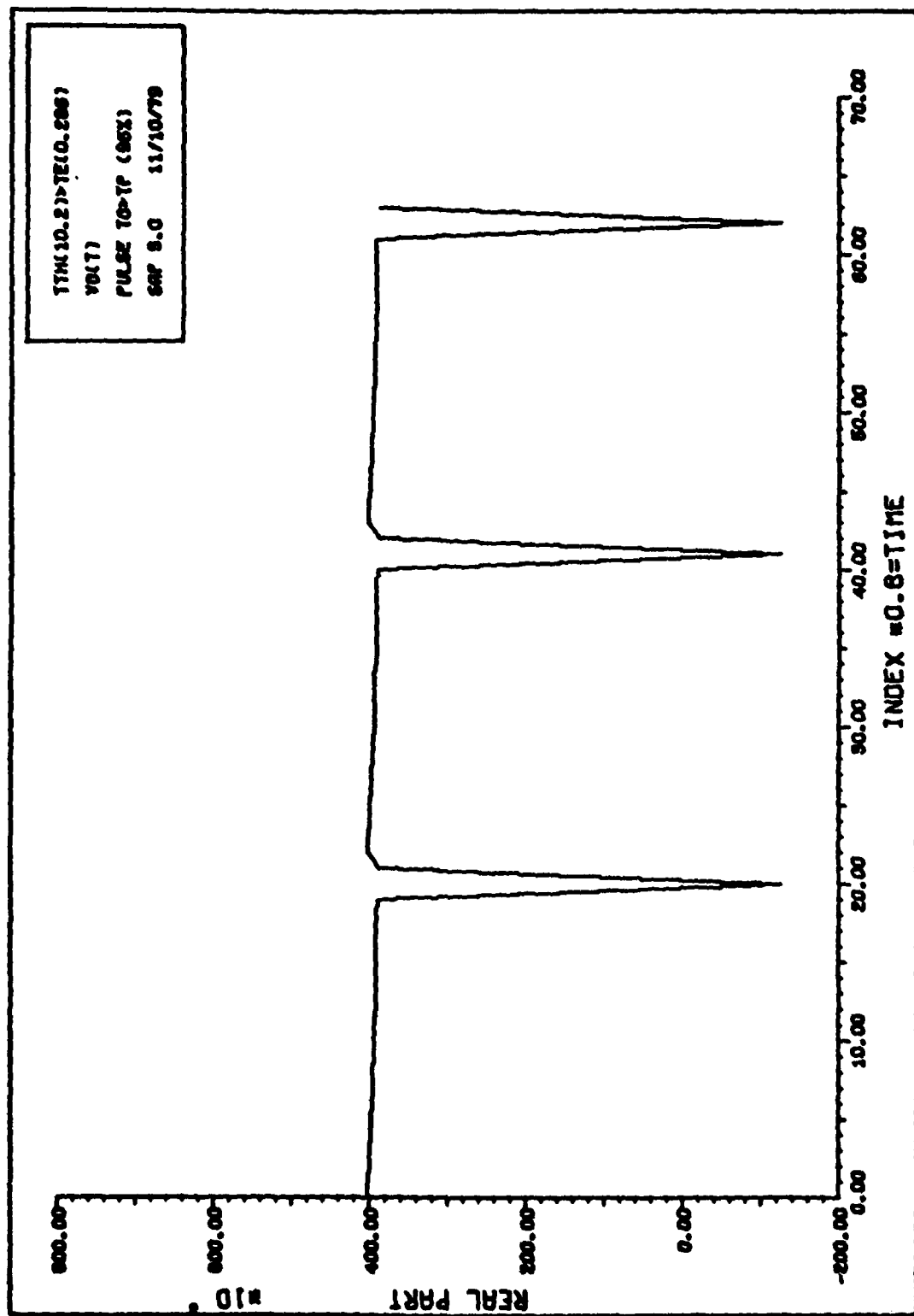


Figure C-8. Pyroelectric Sensor Output Voltage due to a Pulse Train with a 95% duty cycle for $T_{TH} > T_e$ and $t_o > t_p$

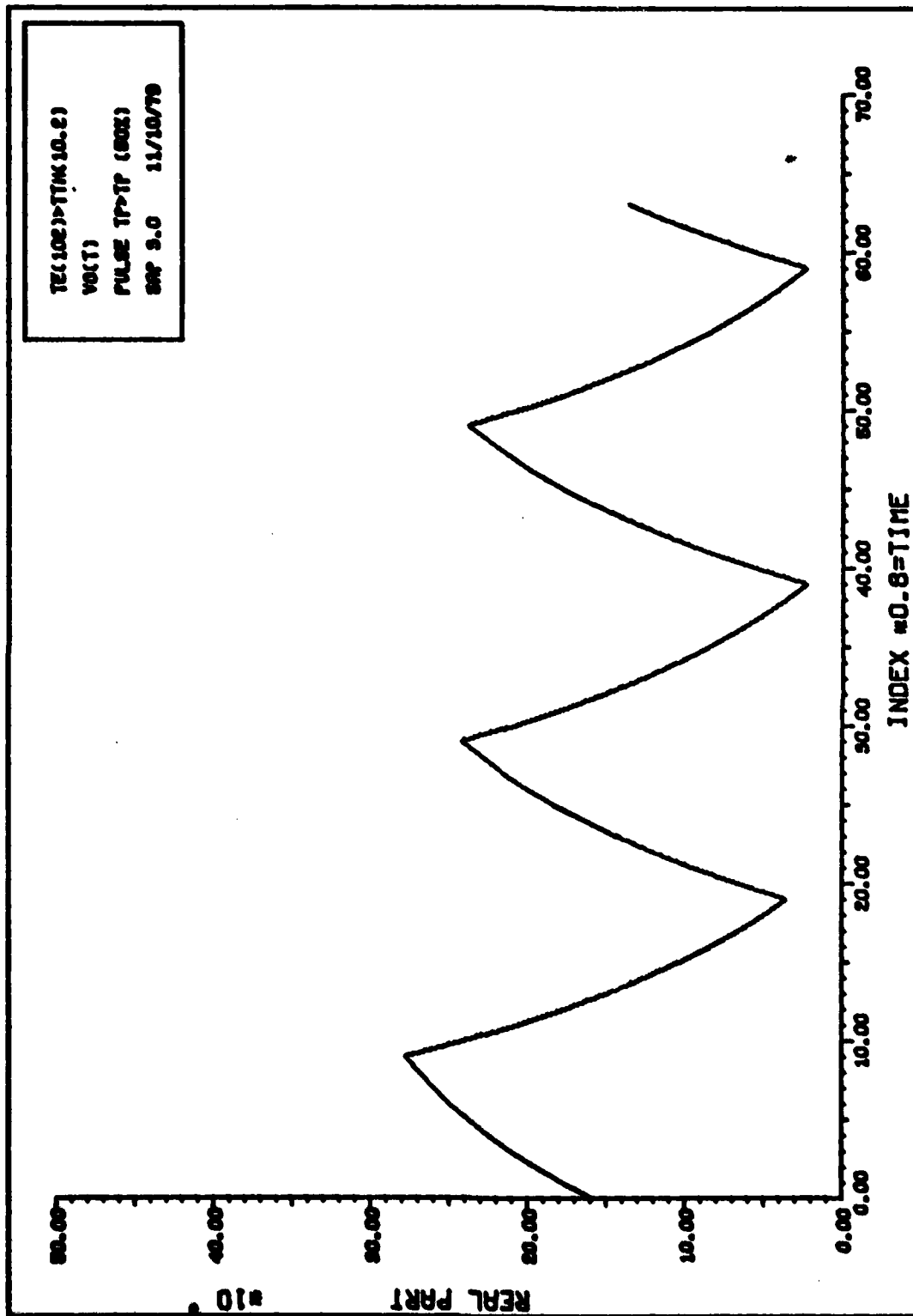


Figure C-9. Pyroelectric Sensor Output Voltage due to a Pulse Train with a 50% duty cycle
 for $T_e > T_{TH}$ and $t_o > t_p$

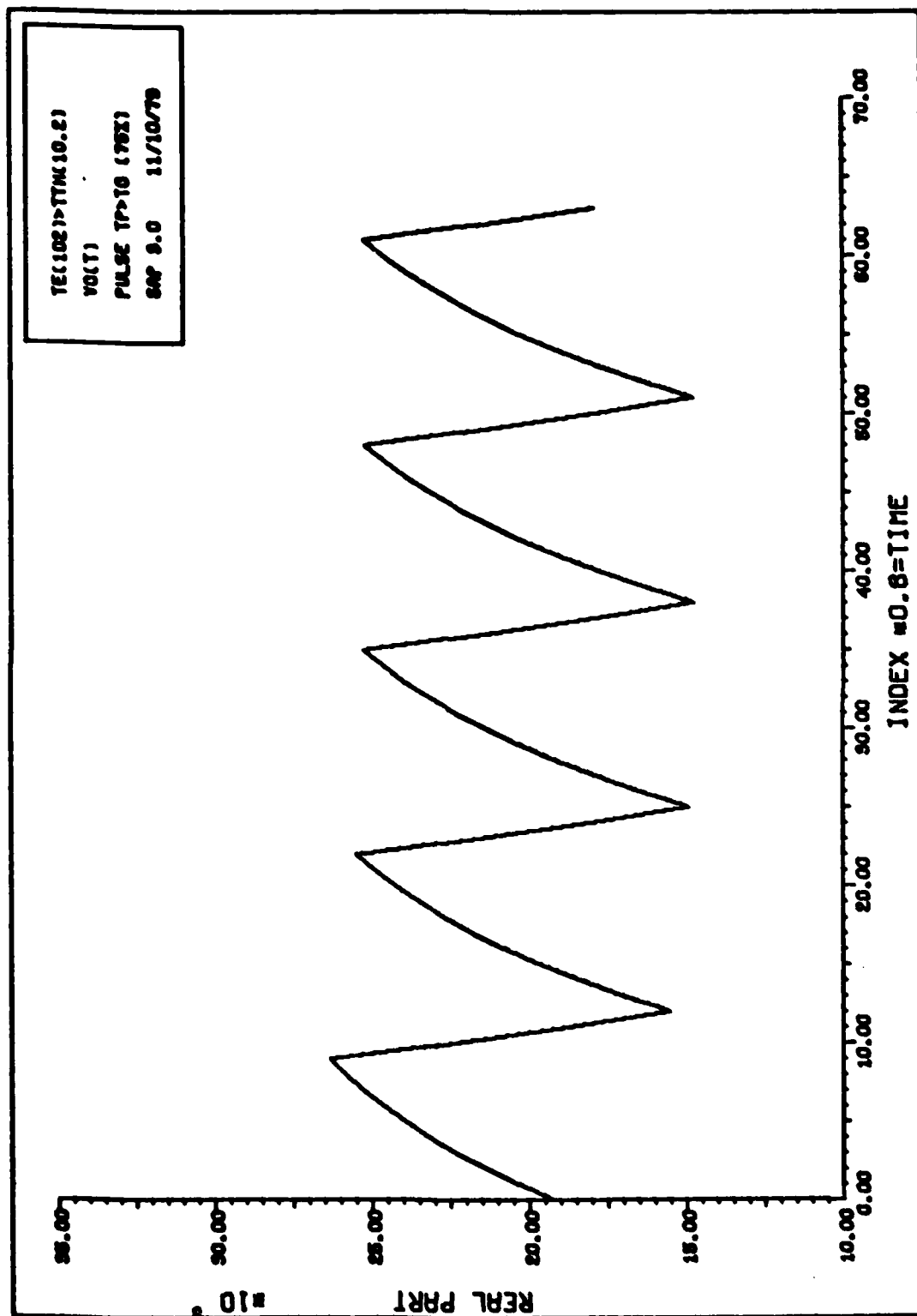


Figure C-10. Pyroelectric Sensor Output Voltage due to a Pulse Train with a 75% duty cycle for $T_e > T_{TH}$ and $t_o > t_p$

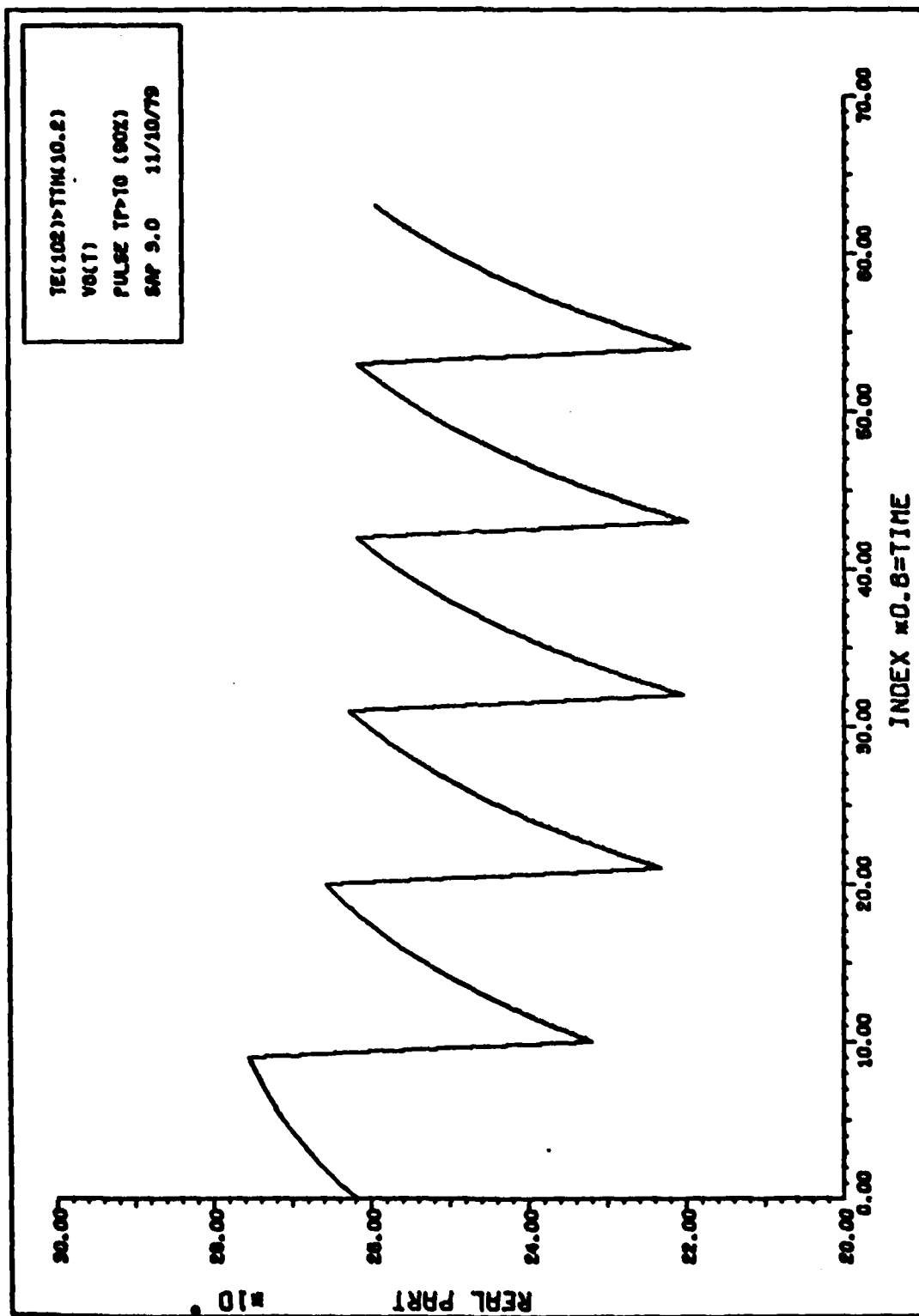


Figure C-11. Pyroelectric Sensor Output Voltage due to a Pulse Train with a 90% duty cycle for $T_e > T_{TH}$ and $t_o > t_p$

VITA

Michael James Goodman was born on 18 April 1956 in Lincoln, Nebraska. He graduated from high school in Arvada, Colorado in 1974 and attended Colorado State University from which he received the degree of Bachelor of Science in Electrical Engineering in May 1978. Upon graduation, he received a commission in the USAF through the ROTC program. His first assignment was at the Air Force Institute of Technology in June 1978. He pursued a Master of Science degree while studying in the graduate Electro-Optics program at the Air Force Institute of Technology.

Permanent Address: 12000 W. 76th Avenue
Arvada, Colorado 80005

UNCLASSIFIED

SECURITY CLASSIFICATION OF THIS PAGE (When Data Entered)

REPORT DOCUMENTATION PAGE		READ INSTRUCTIONS BEFORE COMPLETING FORM
1. REPORT NUMBER AFIT/GEO/EE/79-2	2. GOVT ACCESSION NO.	3. RECIPIENT'S CATALOG NUMBER
4. TITLE (and Subtitle) OPTICAL RECEIVER DESIGN USING PYROELECTRIC DETECTORS		5. TYPE OF REPORT & PERIOD COVERED Thesis
		6. PERFORMING ORG. REPORT NUMBER
7. AUTHOR(s) Michael J. Goodman, B.S. 2nd Lt, USAF		8. CONTRACT OR GRANT NUMBER(s)
9. PERFORMING ORGANIZATION NAME AND ADDRESS Air Force Institute of Technology (ATC) Wright-Patterson AFB OH 45433		10. PROGRAM ELEMENT, PROJECT, TASK AREA & WORK UNIT NUMBERS
11. CONTROLLING OFFICE NAME AND ADDRESS Aeronautical Systems Division/ENAMB Wright-Patterson AFB OH 45433		12. REPORT DATE December 1979
		13. NUMBER OF PAGES 66
14. MONITORING AGENCY NAME & ADDRESS (if different from Controlling Office)		15. SECURITY CLASS. (of this report) UNCLASSIFIED
		15a. DECLASSIFICATION/DOWNGRADING SCHEDULE
16. DISTRIBUTION STATEMENT (of this Report) Approved for public release; distribution unlimited		
17. DISTRIBUTION STATEMENT (of the abstract entered in Block 20, if different from Report)		
18. SUPPLEMENTARY NOTES Approved for public release; IAW AFR 190-17 JOSEPH P. HIPPS, Maj, USAF Director of Public Affairs		
19. KEY WORDS (Continue on reverse side if necessary and identify by block number) Pyroelectric Pyroelectric Detector Optical Receiver		
20. ABSTRACT (Continue on reverse side if necessary and identify by block number) An optical receiver operable over a broad spectral range of the infrared region is possible using a pyroelectric point detector. The pyroelectric detector is modeled as a transducer of thermal radiation to an electrical signal cascaded with an R-C network. The pyroelectric signal is amplified by a preamplifier network. The sensor is, therefore, modeled as a linear bandpass filter. The preamplifier is configured in two modes, the voltage mode which limits— (See Reverse)		

DD FORM 1473

1 JAN 73

EDITION OF 1 NOV 65 IS OBSOLETE

UNCLASSIFIED

SECURITY CLASSIFICATION OF THIS PAGE (When Data Entered)

UNCLASSIFIED

SECURITY CLASSIFICATION OF THIS PAGE(When Data Entered)

the response to a narrow electrical bandwidth, and the current mode which broadens the response over a wide electrical bandwidth. The responsivity bandwidth product is dependent upon the preamplifier components determined by the mode of operation. However, pulse widths and pulse repetition rates can be calculated without regard to mode of operation.

The detector performance is theoretically limited by fluctuations of the incident radiation and is practically constrained by the thermally generated noise within the preamplifier components. The optical receiver signal processing consists of a whitening filter cascaded with a matched filter. The filter network is used to optimally process the sensor output. The processing scheme provides a signal-to-noise improvement of 10^6 over straight detection.

1 million

UNCLASSIFIED

SECURITY CLASSIFICATION OF THIS PAGE(When Data Entered)